Formation conditions and enrichment mechanisms of the Jurassic lacustrine organic-rich shale in the East Fukang Sag, Junggar Basin, NW China: A reassessment based on organic geochemistry

Jinqi Qiao[1,2]*, Qingyong Luo[1,2], Ye Zhang[3,4]*, Dandan Wang[1,2], Hao Cui[1,2], Xiaoqing Shang[5], Luofu Liu[1,2] and Tong Zhang[6]

[1]State Key Laboratory of Petroleum Resources and Prospecting, China University of Petroleum, Beijing, China, [2]School of Earth Sciences, China University of Petroleum, Beijing, China, [3]National Joint Engineering Research Center for Shale Gas Exploration and Development, (Chongqing Institute of Geology & Mineral Resources), Chongqing, China, [4]Key Laboratory of Shale Gas Exploration, Ministry of Natural Resources (Chongqing Institute of Geology & Mineral Resources), Chongqing, China, [5]School of Earth Sciences and Engineering, Xi'an Shiyou University, Xi'an, China, [6]Xinjiang Oilfield Company, PetroChina, Fukang, China

Chemical composition of sediments is often used to evaluate paleoclimate condition, provenance, tectonic setting, depositional condition, and paleoproductivity. However, the validity of these proxies has long been questioned. The comprehensive use of organic and inorganic multi-indicators in combination when interpreting issues related to terrestrial shales should be advocated. The paleodepositional environment, origin of organic matter (OM) and factor controlling OM accumulation in the Early Jurassic Badaowan (J_1b) and Sangonghe (J_1s) as well as Middle Jurassic Xishanyao (J_2x) lacustrine shales in the East Fukang Sag are reassessed by using organic geochemical characteristics of the OM. Some previous knowledge is updated, and some knowledge is further supported by more evidence. The typical clay-rich shale developed under a lacustrine sedimental environment, and the thermal maturity of these organic-rich shales has entered the oil window and formed economic hydrocarbon potential for the tight-oil and shale-oil reservoirs. The paleoclimate conditions of the study area were warm and humid from the Early to Middle Jurassic periods but were colder and drier after the Middle Jurassic period. The salinity of the water column ranged from freshwater to brackish conditions. The J_2x Formation was deposited under oxic conditions, while J_1b and J_1s formations developed under suboxic and reducing environmental conditions. The J_2x Formation OM mainly derived from higher plants was deposited in a terrestrial environment,while the OM of J_1b and J_1s formations was a mixed OM derived from higher plants and bacteria with little algae deposited under bay/estuary environments alternated with terrestrial environments. It is effective to reflect the paleoclimate by element index and judge the salinity by the updated element thresholds, but it is not effective to evaluate the paleoredox conditions by common elemental ratios and to evaluate the paleoproductivity by Ba in the study area.

KEYWORDS

lacustrine organic-rich shale, organic geochemistry, enrichment mechanisms, Fukang Sag, Junggar Basin

1 Introduction

Chemical composition of sediments, i.e., elements including major, trace and rare earth elements, are often used to evaluate paleoclimate conditions, provenances, tectonic settings, depositional conditions (i.e., redox and salinity conditions), and paleoproductivities (e.g., McLennan, 1993; Tribovillard et al., 2006; Zhang et al., 2013; Schoepfer et al., 2015; Shen et al., 2015; Arsairai et al., 2016; Liu et al., 2020; Qiao et al., 2022a and b; Wu et al., 2022a). However, the validity of these proxies has long been questioned. First, some elements are not affected by a single factor and are used to interpret different issues by different scholars, which cannot guarantee a single variable and results in conclusions lacking a single constraint. For example, Cu was used to interpret paleoproductivity, salinity, paleoclimate conditions and hydrothermal activity (Choi and Hariya 1992; Tribovillard et al., 2006; Wu et al., 2022a). Second, the Earth's material composition is not uniform, thereby must result in a wide variation in chemical compositions of different weathering provenance, so the chemical composition of weathering provenance must associate with that of the sediment, but it was always ignored. Third, many elements are enriched in sediments *via* not only abiotic but also biotic processes (Algeo and Maynard, 2004; Tribovillard et al., 2006; Chen et al., 2015a). Considering the above reasons, the information conveyed by the chemical composition of sediments is multiple and complex, especially for the terrestrial lake basins where the ecosystems are relatively fragile. Therefore, it is not sufficient to evaluate the above issues directly through inorganic elements without considering organic matter (OM) itself. Moreover, based on the organic and inorganic indicators, the interpretation of sedimentary environment conditions was often inconsistent. This complexity, as well as uncertainty, is largely rooted in the fact that the chemical composition of sediments is largely determined by a wide variety of factors including the initial weathering provenance composition, transport distance, as well as the processes of weathering, erosion, deposition, and burial diagenesis (Johnsson, 1993). All the time, some scholars tried to improve the reliability of these indicators *via* kinds of methods (Wei and Algeo, 2020; Cao et al., 2021), for instance, the proposal of the enrichment factor (EF) (Algeo and Maynard, 2004; Tribovillard et al., 2012). However, this cannot solve the above problems once and for all. Algeo and Liu (2020) as well as Algeo and Li (2020) argued that some common parameters, e.g., V/(V+Ni), V/Cr, and Ni/Co, are not valid based on thresholds proposed by Jones and Manning (1994) and advocated for the discontinuation of these indicators. Since sedimentary environments and OM enrichment mechanisms act directly on and are reflected in OM, the joint use of organic and inorganic indicators when interpreting issues related to terrestrial shales should be advocated.
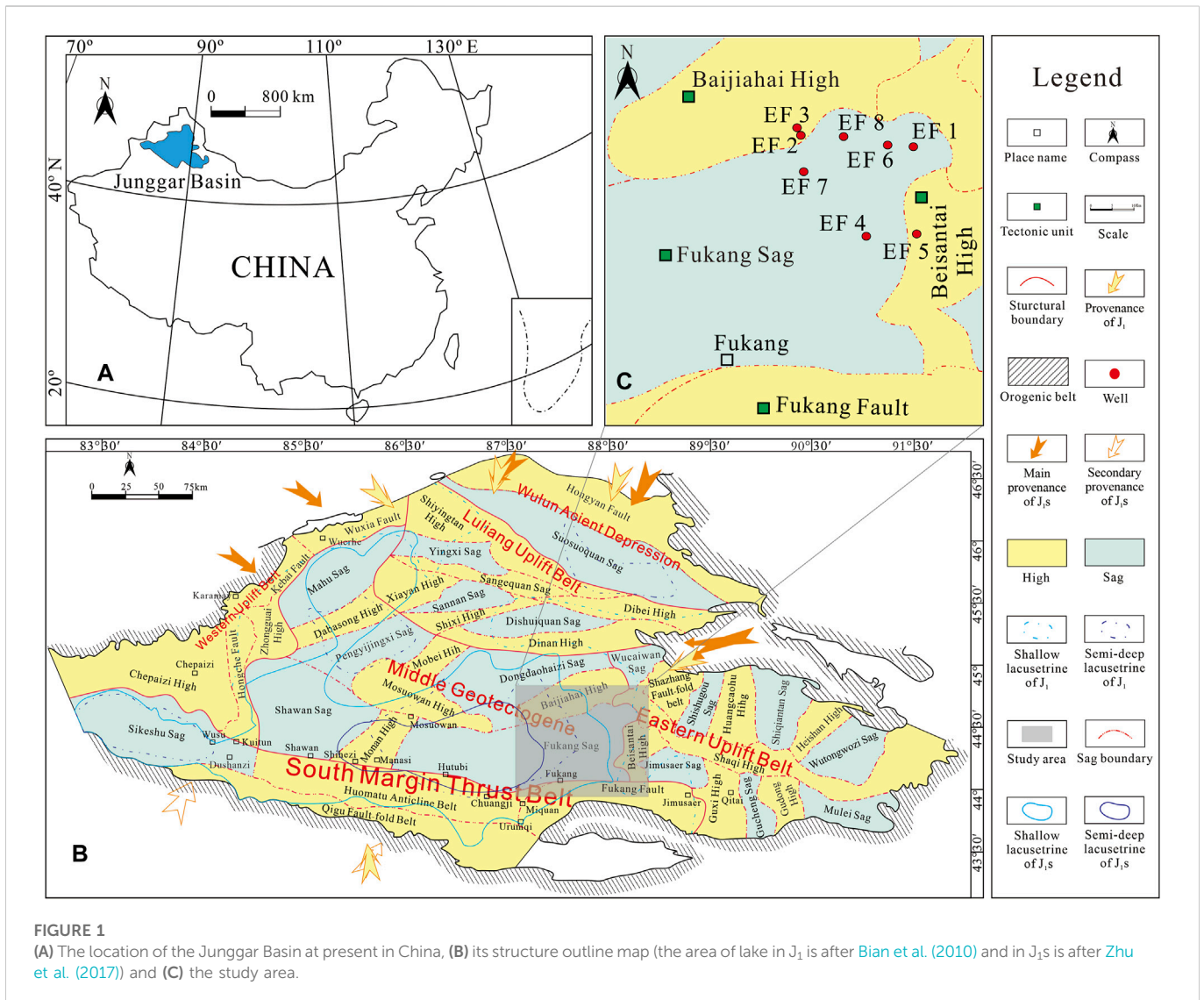
The Fukang Sag is one of the most important sags in the Junggar Basin. It developed three sets of lacustrine shales during the Jurassic period, i.e., the Early Jurassic Badaowan (J_1b) and Sangonghe (J_1s) formations as well as the Middle Jurassic Xishanyao (J_2x) Formation. These shales are low-mature and mature with significant hydrocarbon generation potential at present (cf. Qiao et al., 2020). Qiao et al. (2020) interpreted the paleoclimate condition, depositional environment condition, palaeoproductivity and OM accumulation mechanism based on major and trace elements. However, these evaluations lack more direct and valid evidence derived from organic geochemistry. This paper focuses on the OM in these Jurassic lacustrine shales in the East Fukang Sag. Paleodepositional environments, origins of OM and factors controlling OM accumulation are reassessed by evaluating the geochemical characteristics of these OM and more effective indicators. Some previous knowledge is updated, and some knowledge is further supported by more evidence.

2 Geological setting

The Junggar Basin, which is a typical Upper Palaeozoic, Mesozoic, and Cenozoic superimposed basin, covers an exploration area of around 130,000 km^2 in NW China (Chen and Shi, 2003; Cheng et al., 2022; Figure 1A). The basement is combined by the Precambrian crystalline and part of the Hercynian folded basement. The tectonic evolution can be divided into four stages which are a marine and residual marine foreland basin during the Late Carboniferous-Early Permian period, a continental foreland basin during the Middle-Late Permian period, an intracontinental oscillatory depression basin during the Mesozoic period, and a regeneration foreland basin during the Cenozoic period (Cao et al., 2005; Chen et al., 2015b). These tectonic evolutions were controlled by multiphase tectonic cycles including the Hercynian, Indosinian, Yanshanian and Himalayan orogenic events (Wan et al., 2015).

The Fukang Sag is the largest hydrocarbon-generating sag in the basin, which is surrounded by the Beisantai High and Shazhang Fault-fold Belt to the east, the Huomatu Anticlinal Belt and Fukang Fault Zone to the south, the Monan High to the west, and the Baijiahai High and Mosuowan High to the north at present (Figure 1B). The sag is located in the central depression belt of the basin presently (Figure 1B) and is characterized by a NE-SW-trending monocline (Cao et al., 2017a; and b; Figure 1C) with a dip angle of <3° under the effects of the rapid initial uplift during the Early Jurassic and slow uplift during the Middle Jurassic on the southern margin of the basin, respectively. The stratigraphic successions in the Fukang Sag cover from the Carboniferous to the Quaternary deposits with the largest thickness of roughly 10 km, in which the Carboniferous, Permian, Triassic, and Jurassic successions developed organic-rich shales (Chen et al., 2003a; 2003b). The Jurassic strata can be subdivided into five units including the J_1b, J_1s, J_2x, Toutungou (J_2t), and Qigu (J_3q) formations based on stratigraphic contact, lithological association and sedimentary cycle. The investigated area developed a shallow intracontinental lacustrine setting with depositional faces of lacustrine, deltaic, fluvial, and alluvial fan under a low-amplitude oscillating tectonic setting during the Early to early Middle Jurassic period (the J_1b, J_1s, and J_2x formations) (e.g., Cao et al., 2017b). The lithology of the J_1b, J_1s and J_2x formations is mainly composed of coal seam, organic-rich shale, siltstone, conglomerate, and sandstone (Figure 2). Then, the scale of the lacustrine area shrank rapidly because of the Early Yanshanian orogeny (Cao et al., 2017b) during the late Middle-Late Jurassic periods. These periods developed three depositional faces including shallow lacustrine, fluvial, and deltaic facies characterized by the successions with lithology dominated by organic-rich shales, siltstone, and sandstone (the J_2t and J_3q formations). Most of the faults are NE-trending and E-W-trending normal faults, which are confined to the Jurassic strata (Cao et al., 2017a). The fault throws are generally ranging from tens to hundreds of meters and the strike length is <2 km.

FIGURE 1
(A) The location of the Junggar Basin at present in China, **(B)** its structure outline map (the area of lake in J_1 is after Bian et al. (2010) and in J_1s is after Zhu et al. (2017)) and **(C)** the study area.
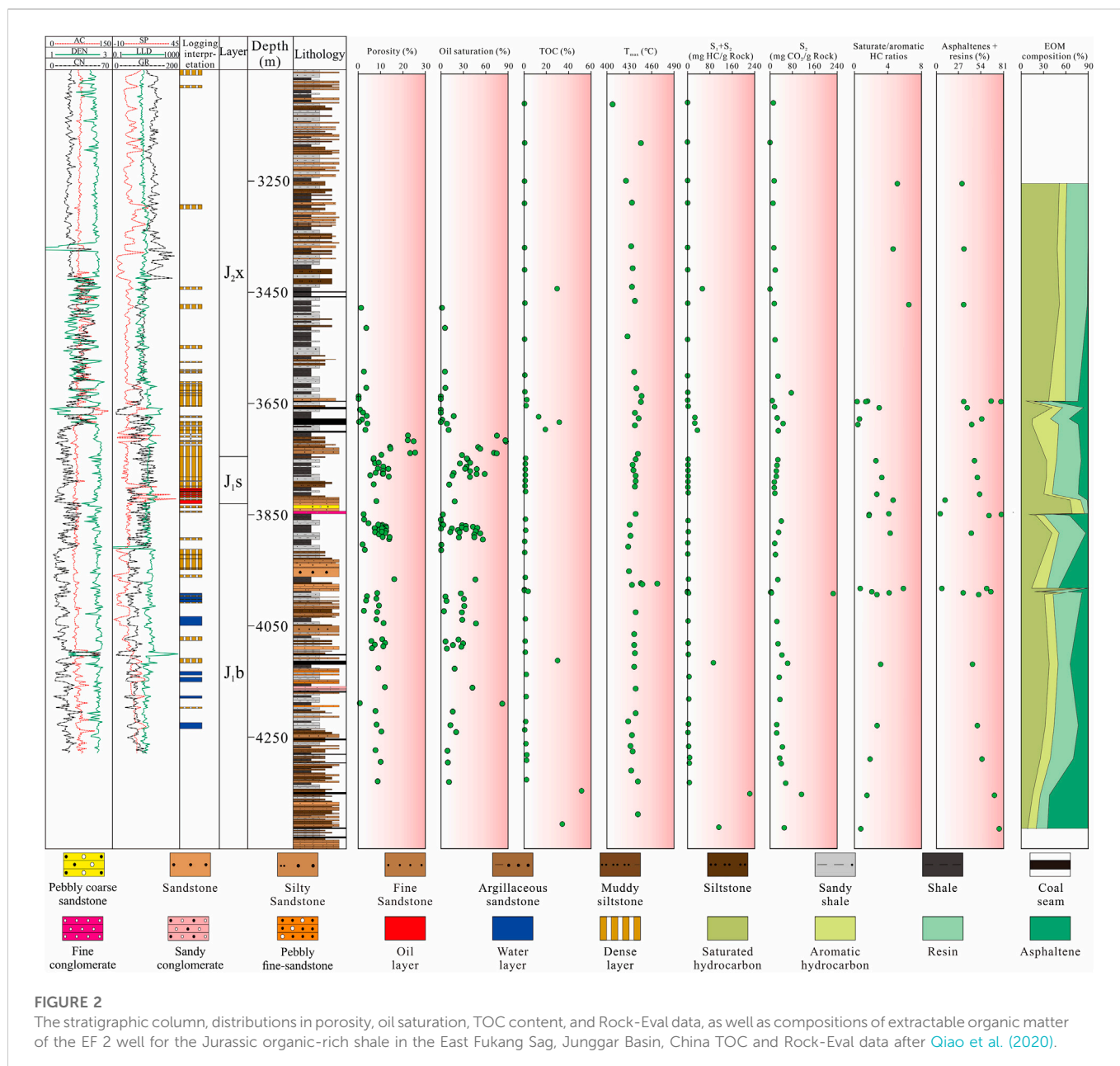
3 Sampling and analytical methods

3.1 Samples and data

The studied samples came from the same wells discussed in Qiao et al. (2020). 80 samples were used to perform hydrocarbon extraction and fractionation as well as quantification of each compound and gas chromatography-mass spectrometry (GC-MS) analysis. 37 saturated hydrocarbon fractions were used to perform gas chromatography-flame ionization detector (GC-FID), and stable carbon isotope composition ($\delta^{13}C$) for all fractions was performed in 25 samples. Moreover, clay minerals compositions from 232 samples as well as porosity and oil saturation data from 83 samples that came from EF 2 well were provided by the Xinjiang Oil Field.

3.2 Hydrocarbon extraction and fractionation

Before the test, all analyzed samples were pulverized with a size of <80 mesh to obtain extractable OM (EOM) (i.e., saturated hydrocarbons, aromatic hydrocarbons and resins) by using a

Soxhlet extractor system (SEM) with a solvent of dichloromethane (DCM). After the extraction, the addition of activated copper powder and anhydrous sodium sulfate, in turn, to the EOM achieved the removal of water and elemental sulfur, respectively.

The solvents were evaporated to near dryness at below 40°C and then removed into triangular bottles. Adding *n*-hexane with constant shaking, then performing ultrasonic dissolution. The asphaltene was entirely precipitated after a static settlement for more than 12 h. Then the material was removed to a short-necked funnel stuffed with skimmed cotton and washed with *n*-hexane until the filtrate was colorless to obtain the EOM which was distilled to 2–3 mL. The asphaltene remained in the short-necked funnel, cotton and triangular bottle was dissolved and washed with DCM until the filtrate was colorless. The EOM composition was eluted with *n*-pentane for aliphatic hydrocarbon compounds, a mixture solvent of *n*-pentane and DCM (2:3; V:V) for aromatic hydrocarbon compounds, and methanol for resin compounds, in turn, by using a silica gel (activation in an electric drying oven at 200°C for at least 4 h)-Al_2O_3 (activation in an electric drying oven at 400°C–450°C for at least 4 h) chromatography. The separated saturated and aromatic hydrocarbon components were volatilized to dry at the condition

FIGURE 2
The stratigraphic column, distributions in porosity, oil saturation, TOC content, and Rock-Eval data, as well as compositions of extractable organic matter of the EF 2 well for the Jurassic organic-rich shale in the East Fukang Sag, Junggar Basin, China TOC and Rock-Eval data after Qiao et al. (2020).

of <40°C, and the resin and asphaltene components were volatilized to dry at the condition of <60°C.

After the solvent in remnants was evaporated to dryness, the weight difference between the two weighing intervals of 30 min of <0.3 mg can be regarded as constant weight.

3.3 Analyses of molecular geochemistry and carbon isotopes

n-alkanes and isoprenoids in the saturated hydrocarbons were analyzed by GC-FID, while terpanes (m/z = 191; Figures 3A,C) and steranes (m/z = 217; Figures 3B,D) in saturated hydrocarbons, as well as aromatic hydrocarbons including methylphenanthrenes (MPs, m/z = 194; Figure 3E), trimethylphenanthrenes (TMPs, m/z = 220;

Figure 3F), chrysene (m/z = 228; Figure 3G), and triaromatic steroid (TMPs, m/z = 231; Figure 3H), were performed by GC-MS.

The instrument of GC-FID was Shimadzu GC-2010 (Japan) equipped with HP-5MS chromatographic column (30 m × 0.25 mm × 0.25 μm). The carrier gas was 99.999% helium at a velocity of 1.0 mL/min. The inlet temperature was 300°C and the split ratio was 50:1. During the analysis, the initial temperature of the GC oven was 100°C for 1 min, then programmed to raise to 300°C at 4°C/min and hold for 25 min. The temperature of the FID was 300°C with hydrogen of 40 mL/min and air of 400 mL/min.

The instrument of GC-MS was Agilent 7890GC/5977MS (America) equipped with HP-5MS chromatographic column (the stationary phase consists of 95% poly (methylsilicone) and 5% poly (phenylmethylsilicone); 30 m × 0.25 mm × 0.25 μm). The carrier gas was 99.999% helium at a velocity of 1.0 mL/min. During the analysis,
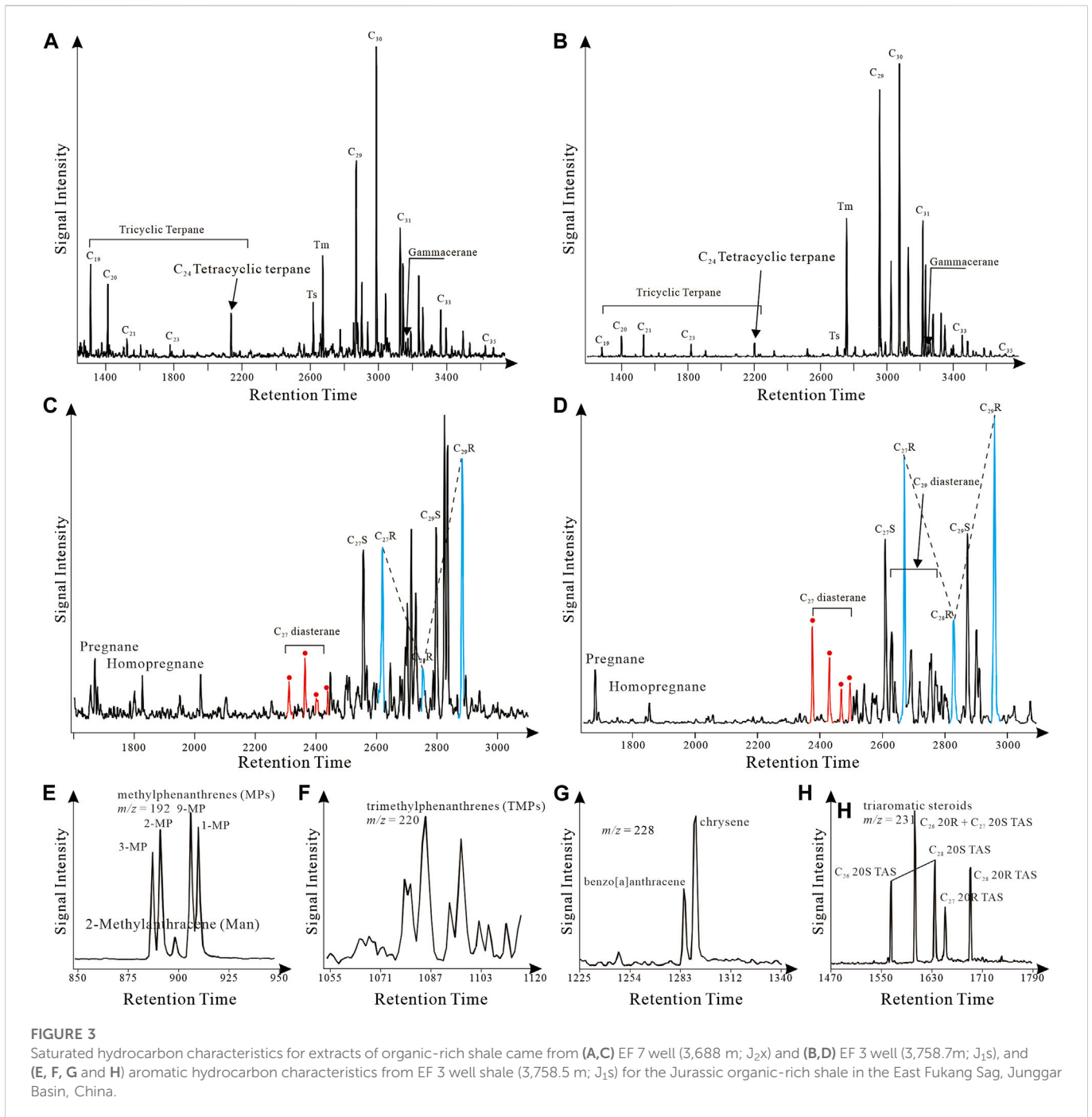
FIGURE 3
Saturated hydrocarbon characteristics for extracts of organic-rich shale came from **(A,C)** EF 7 well (3,688 m; J_2x) and **(B,D)** EF 3 well (3,758.7m; J_1s), and **(E, F, G** and **H)** aromatic hydrocarbon characteristics from EF 3 well shale (3,758.5 m; J_1s) for the Jurassic organic-rich shale in the East Fukang Sag, Junggar Basin, China.

the initial temperature of the GC oven was 100°C for 1 min, then programmed to raise to 300°C at 4°C/min and hold for 20 min. The MS was performed in electron ionization (EI⁺) mode with an ion source temperature of 230°C and ionization energy of 70 eV.

The relative abundance of each compound was calculated from the peak area, and the identification of compounds was based on their relative retention time compared with literature data (e.g., Wu et al., 2022b; Zheng et al., 2022).

The measurement of $\delta^{13}C_{org}$ was performed using a gas isotope ratio mass spectrometer (Finnigan MAT-252) equipped with a 30 m Porapak Q chromatographic column with 20 μm film thickness. The carrier gas was 99.999% helium at a velocity of 1.2 mL/min. During the

analysis, the initial temperature was 40°C for 1 min, then programmed to raise to 160°C at 15°C/min. The $\delta^{13}C_{org}$ value was calculated by comparing it to the intentional PDB (Pee Dee Belemnite) standard, and the analytical error was ±0.1‰.

4 Results and discussion

4.1 Origins of organic matter

The kerogen type for the examined samples has been interpreted based on the results from maceral composition, Rock-Eval pyrolysis,
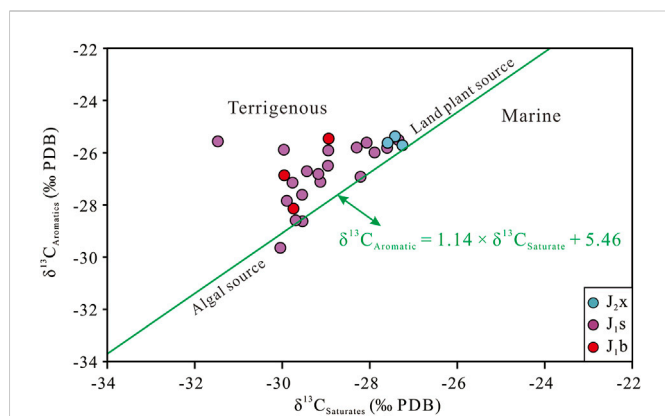
FIGURE 4
$\delta^{13}C_{Saturate}$ vs $\delta^{13}C_{Aromatic}$ for the extractable organic matter from the Jurassic organic-rich shale in the East Fukang Sag, Junggar Basin, China. The green line is the best fit separation for waxy and non-waxy hydrocarbons (Sofer, 1984).
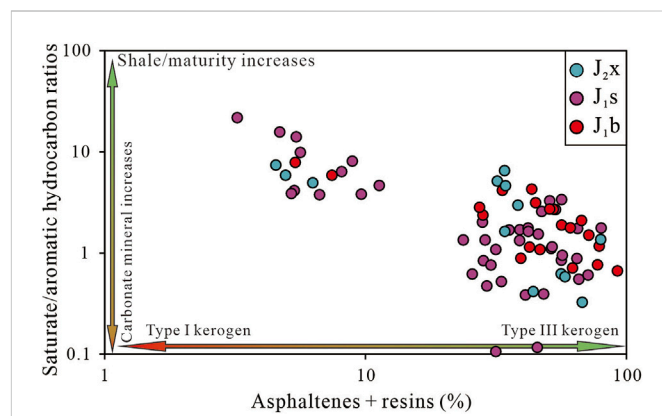

FIGURE 5
Saturate/aromatic hydrocarbon ratios vs asphaltenes + resins concentrations showing the depositional setting, maturity and kerogen type of the Jurassic organic-rich shale in the East Fukang Sag, Junggar Basin, China.

and atomic ratios of isolated kerogen (i.e., H/C, O/C and C/N) (Qiao et al., 2020). The kerogen type was generally interpreted as type III kerogen, although there are large differences based on the indicators mentioned above (cf. Figure 7 in Qiao et al., 2020). So, it is necessary to use more parameters to interpret the OM origins.

The stable carbon isotope ($\delta^{13}C$) compositions of the saturated hydrocarbon fraction ($\delta^{13}C_{Sat.}$) in the analyzed J_1b, J_1s and J_2x OM-rich shales vary from –28.95 to –29.97‰, –27.35‰ to –31.49‰, and –27.26‰ to –27.60‰, respectively; and of the aromatic fraction ($\delta^{13}C_{Aro.}$) from –25.47 to –28.46‰, –25.52‰ to –29.67‰, and –25.38‰ to –25.72‰, respectively. The $\delta^{13}C_{Sat.}$ and $\delta^{13}C_{Aro.}$ compositions of the investigated shales plotted on the Sofer (1984) diagram showing that all these extracts originated from shales that received predominatly terrestrial land plants (Figure 4). Another parameter, i.e., Canonical Variable (CV $= - 2.53 \times \delta^{13}C_{Sat.} + 2.22 \times \delta^{13}C_{Aro.} - 11.65$) (Sofer, 1984), can be used to discriminate OM from terrigenous and marine settings. Values of >0.47 indicate predominantly non-waxy terrigenous organic sources, whereas of <0.47 indicate more contribution from marine OM (Sofer, 1984; El Diasty et al., 2016). The calculated CV values for the studied samples ranging from –0.47 to –11.25 with 80% of >0.47 indicate that the OM was derived from terrestrial settings, and the samples below the threshold are likely to be affected by maturity (Collister and Wavrek, 1996) and caused by higher salinity mentioned later. Moreover, the CV values indicate the stratifications in water columns as well (Collister and Wavrek, 1996). The terrestrial OM can be further supported by the depleted $\delta^{13}C$ values which are gradually increasing from the saturated hydrocarbon to the aromatic hydrocarbon, then to the resins ranging from –28.94‰ to –25.41‰ (avg. –26.68‰) and finally to the asphaltene ranging from –28.82‰ to –24.61‰ (avg. –26.31‰) (Galimov, 2006). The type III kerogen can be further supported by the relative concentrations of the asphaltenes and resins (from 3.2% to 92.4% and 39.4% on average, of EOM) compared to the concentrations of aliphatic and aromatic hydrocarbons (Figure 5).

Biomarkers, as indicators of parent sources of OM, have been widely used (Luo et al., 2016; Wu et al., 2022b; Zheng et al., 2022; Zhu et al., 2022). The distribution pattern of saturated hydrocarbons

contains a lot of information on biological sources. *n*-alkanes with low carbon numbers (i.e., *n*-C_{12}–C_{18}) mainly originate from phytoplankton and algae (Meyers, 1997; Luo et al., 2016). Short-chain *n*-alkanes with relatively high concentrations of C_{17} or C_{18} typically originate from marine algae and cyanobacteria (Riboulleau et al., 2007; Sachse and Sachs, 2008). Middle-chain *n*-alkanes (*n*-$C_{21–25}$) are sourced from aquatic higher plants in common (Ficken et al., 2000), especially with peak carbon of *n*-C_{23} and *n*-C_{25} alkanes (Huang et al., 1999) being inductive of aquatic pollen taxa, Nymphaea (Coetzee, 1967), Sphagnum moss species (Nichols et al., 2006; Bingham et al., 2010), fresh-water algae (Riboulleau et al., 2007). Furthermore, long-chain *n*-alkanes with obvious odd carbon predominance are generally input of higher plants (Eglinton and Calvin, 1967) and the high concentrations of C_{27}, C_{29}, and C_{31} *n*-alkanes are indicative of the land plant epicuticular waxes (Meyers, 1997). Based on the above indicative information, the parent material source of OM can be interpreted. The Paq values ranging from 0.36 to 0.90 (avg. 0.68) indicate aquatic macrophytes make an important contribution to OM (Ficken et al., 2000). The moderate to high WI values of 0.70–4.50 (avg. 1.91) in most samples indicate a substantial contribution of terrestrial OM. The CPI values of the investigated samples here are consistent with terrestrial OM input based on the consideration of the maturity stage. Additionally, the occurrence of branched alkanes indicates a contribution from bacteria to OM (Shiea et al., 1990). For example, the appearance of farnesane (*i*-C_{15}) indicates the input of green sulfur bacteria (Summons and Powell, 1987). The concentrations of branched alkanes (e.g., *i*-C_{15}/*n*-C_{13} are 0–2.57 with an average value of 0.33; *i*-C_{16}/*n*-C_{14} are 0–2.52 with an average value of 0.52; *i*-C_{17}/*n*-C_{15} are 0–2.89 with an average value of 0.24) indicate the contribution from bacterial was abundant.

However, it must be noticed that these results drawn from the distribution of *n*-alkanes distributions should be used with caution, because the longer the carbon chain, the easier it is to convert to shorter chains with increasing maturity and thus change its distribution pattern (Peters et al., 2005) and the biological source signal based on *n*-alkanes is not exclusive (Oros et al., 1999; Gonzales et al., 2020).

Steranes are mainly derived from higher plants (e.g., a high concentration of C_{29} steranes) and algae (e.g., a predominance of
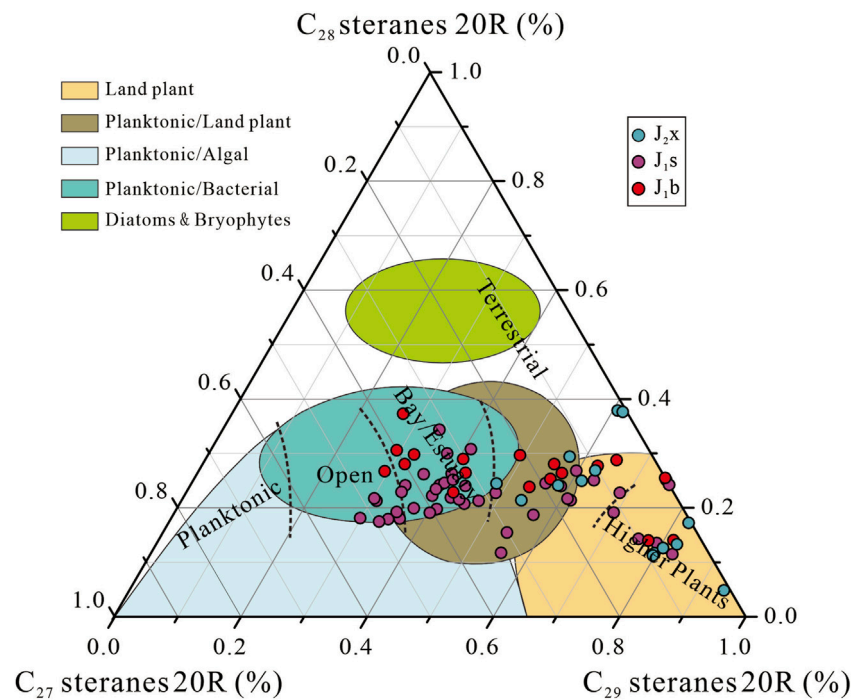
FIGURE 6
Ternary diagram showing the distribution of C_{27}, C_{28} and C_{29} steranes and the Jurassic organic-rich shales' depositional environment in the East Fukang Sag, Junggar Basin, China (modified after Huang and Meinschein, 1979; Moldowan et al., 1985).

C_{27} steranes) (Huang and Meinschein 1979; Moldowan et al., 1986; Volkman 2003), and hopane sources are mainly from aerobic bacterial membranes (Ourisson and Rohmer, 1992; Peters et al., 2005). The low steranes/hopanes ratio ranging between 0.07 and 2.98 with an average value of 0.37 indicates a substantial input of bacterial biomass.

The ternary diagram of C_{27}, C_{28} and C_{29} $\alpha\alpha\alpha$ 20R steranes distributions (Figure 6; Huang and Meinschein 1979) indicates that the OM of the J_2x Formation sourced mainly from higher plants was deposited in a terrestrial environment, while the OM of the J_1 formations (i.e., J_1b and J_1s formations) was a mixed OM derived from higher plants, bacteria and algae deposited under bay/estuary environments alternated with a terrestrial environment (Figure 6). Moreover, the presences of abundant TMPs and chrysene (Figure 3F), etc. are typically indicative of terrigenous higher plant input (Chaffee and Johns 1983; Chaffee and Fookes 1988).

4.2 Paleodepositional environment

Based on the lithology assemblage (Figure 2), a typical lacustrine sedimental environment can be recognized. The lithology enriched in clay minerals was deposited in a non-restricted setting, which can be demonstrated by the high C_{27} diasteranes abundances compared to regular steranes, but low C_{21-22} steranes abundances compared to C_{27-29} steranes (Figure 7) (Wang et al., 2015; Qiao et al., 2021a; Zheng et al., 2022). Clay-rich lithology is further supported by the higher C_{30} hopane abundance compared to the lower C_{29} hopane abundance (Figure 3) with the C_{29}/C_{30} hopane of 0.41–1.50 (0.68 on average) (Gürgey, 1999). This is consistent with the distribution of gradually regular decrease from C_{31} to C_{35} hopanes indicating clastic facies
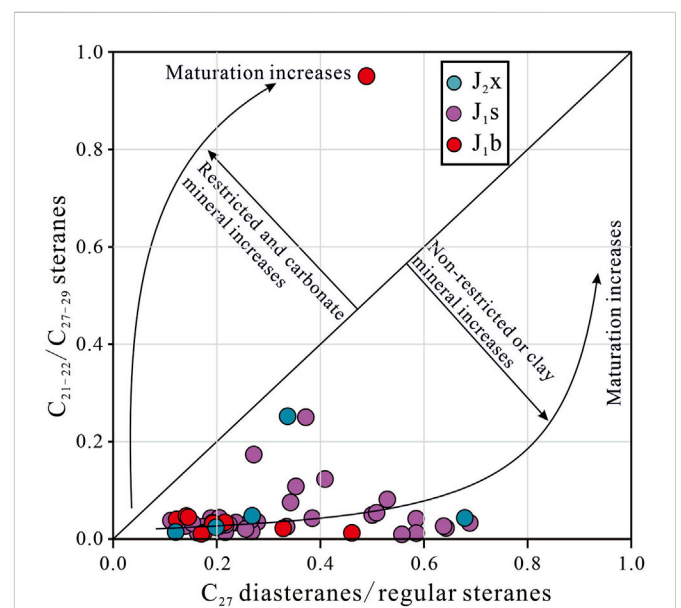
FIGURE 7
Plot of C_{21-22}/C_{27-29} steranes vs C_{27} diasteranes/regular steranes, showing the depositional setting of the Jurassic organic-rich shale in the East Fukang Sag, Junggar Basin, China (modified after Wang et al., 2015).

(Figure 3; Waseda and Nishita, 1998), the C_{26}/C_{25} Tri (tricyclic terpane) (0.81–3.30 with an average value of 1.89) and C_{34}/C_{35} hopane (1.02–4.35) ratios, low C_{22}/C_{21} (0–1.08 with an average value of 0.25) and C_{24}/C_{23} Tri ratios (0–6.21 with an average value

FIGURE 8
(A) C_{24}/C_{23} vs C_{22}/C_{21} tricyclic terpane and **(B)** $C_{31}R/C_{30}$ hopane vs C_{26}/C_{25} tricyclic terpane of the Jurassic organic-rich shale in the East Fukang Sag, Junggar Basin, China (modified after Peters et al., 2005).
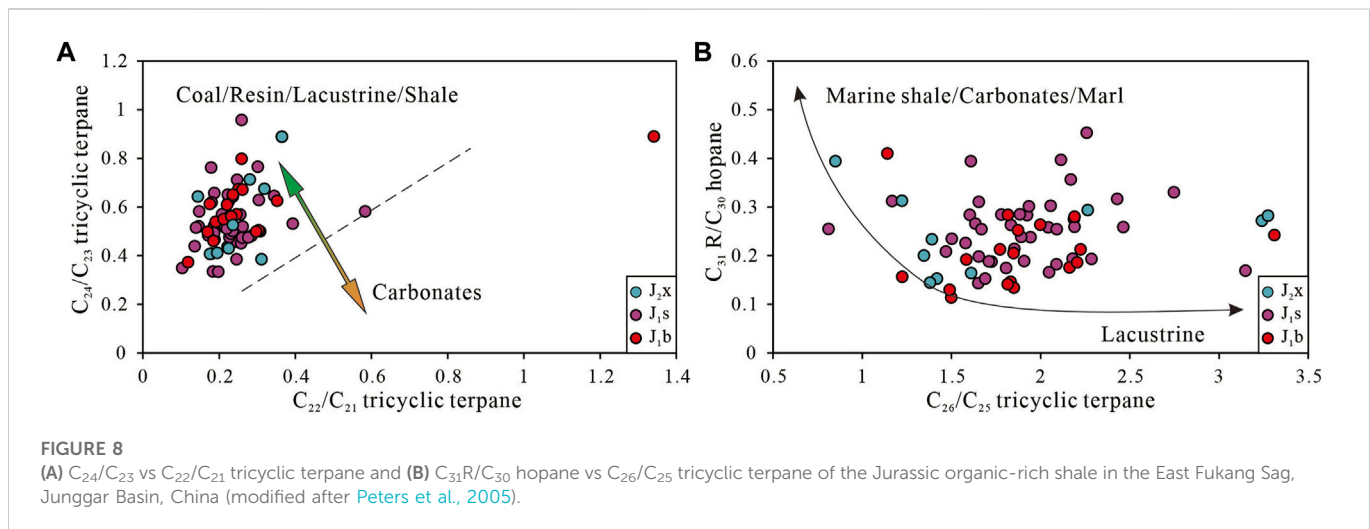
of 0.63), as well as low HHI values (0–0.10) (Peters and Moldowan, 1991; Sinninghe Damsté et al., 1995; Peters et al., 2005) (Figure 8). Non-marine setting can be supported by the high ratios of C_{30} hopane/(20R steranes + C_{30} hopane) ranging between 0.18 and 0.83 (avg. 0.66) (Holba et al., 2003). The lacustrine depositional environment can be also supported by the low steranes abundances compared to hopanes in all formations (0–0.95 with an average value of 0.06) (Peters et al., 2005). Considering that steranes abundances would also be high in lacustrine settings which developed plenty of biomass inputs, the low steranes abundances in the studied area are consistent with the OM compositions discussed above.

However, the parameter of C_{31} 22R/C_{30} hopane ratios (0–0.52 with an average value of 0.25) (Figure 8B), which is inductive of marine situations at the situation of ratio >0.25 and lacustrine environments at of <0.25 (Peters et al., 2005), is inconsistent with the above discussion for the analyzed samples, which might be due to the paleosalinity conditions.
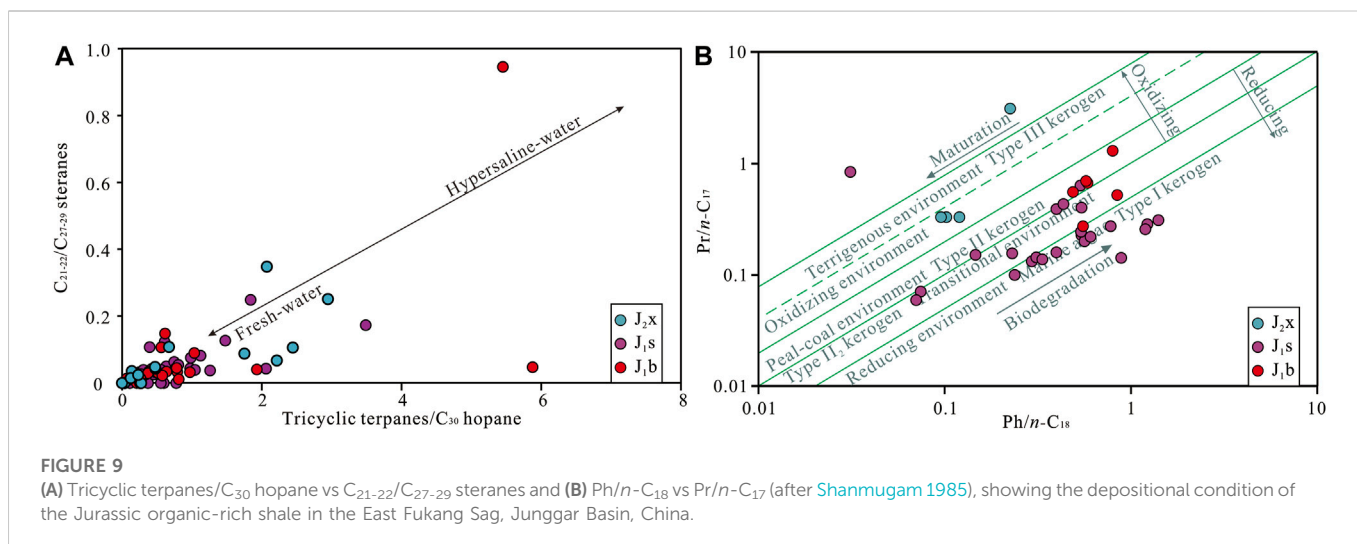
4.2.1 Paleosalinity conditions

Generally, salinity is more changeable in lake systems, which affects the community composition of the aquatic organism (Romero-Viana et al., 2012). Qiao et al. (2020) released some trace and rare earth elements to discuss the palaeosalinity conditions of the J_2x, J_1s and J_1b formations based on the thresholds published by some early literature, which illustrated that the J_1 and J_2x formations were deposited under a fresh-water condition. However, some new thresholds have been proposed by Wei and Algeo (2020), where B/Ga is <3 in freshwater, with a value of 3–6 indicative of brackish, and transition from brackish to marine facies occurs at B/Ga ratio of 6; and Sr/Ba of <0.2 corresponds to freshwater, 0.2–0.5 to brackish, and >0.5 to marine facies. The new thresholds show a completely different conclusion, which indicates the most studied samples developed under freshwater conditions (65.8% and 68.5% based on Sr/Ba and B/Ga, respectively), some formed under brackish (23.3% and 15.1%) and a few under marine environments (11.0% and 16.4%).

The large variations of the Tris/C_{30} αβ hopane (0–5.88) and (pregnane + homopregnane)/steranes ratios (0–0.95), as well as the occasional appearance of β-Carotane, also deduce the lacustrine

environment with changeable salinity (Kruge et al., 1990; Peters et al., 2005) (Figure 9A). The same result is further supported by 59% of the C_{30} hopane/(20R steranes + C_{30} hopane) ratios being smaller than 0.7 (Holba et al., 2003). The existence of gammacerane indicates the thermal and saline stratifications in water columns in lacustrine environments (Sinninghe Damsté et al., 1995). Gammacerane originates from tetrahymanol and is synthesized by bacterivorous ciliates that feed at the redox interface of the stratified water columns (Sinninghe Damsté et al., 1995). The wide range of gammacerane abundances with the gammacerane/C_{30} hopane ratios ranging between 0 and 0.3 is consistent with the above inferences on the salinity change and stratifications (e.g., the CV values in Section 4.1) in lacustrine environments. Additionally, the above discussion also proves that the thresholds proposed by Wei and Algeo (2020) are more reliable than those by earlier literature. The variation of salinity is consistent with the appearance of the brackish-water bivalve Waagenoperna in the J_1b Formation of the Junggar Basin (Pan et al., 2013).

4.2.2 Paleoredox conditions

Besides paleosalinity, OM preservation and paleoproductivity are affected by paleoredox situations (Katz, 2001). Pr/Ph ratio is an important parameter for paleoredox conditions (Didyk et al., 1978; Zhang et al., 2020; Wu et al., 2022b; Zheng et al., 2022). In general, Pr/Ph is >3 indicating oxic environments at the benthic water column with substantial contributions from higher plants, whereas Pr/Ph is <1 in anoxic situations with increasing input of algae (Didyk et al., 1978). The paleoenvironments with the shallower water column and more oxidation degree (e.g., marshes, wetlands, paralic etc.), the higher ratio of Pr/Ph. For the analyzed samples from the J_2x Formation, most of them show the ratio of Pr/Ph being >3, indicating oxic environments. For the J_1s samples, Pr/Ph ratios of 60% are between 1 and 3 and of 30% are <1, indicating suboxic environment conditions in most cases with some reducing environments. By contrast, Pr/Ph ratios of 66% from the J_1b Formation are <1 and no ratios are >3 indicating least reducing situations (Didyk et al., 1978; Peters et al., 2005). Additionally, the oxic conditions of the water column for the J_2x Formation are further supported by the plot of Pr/n-C_{17} vs Ph/n-C_{18} (Figure 9B). However, the bivariate plot of Pr/n-C_{17} vs Ph/n-C_{18} indicates the paleoredox

FIGURE 9
(A) Tricyclic terpanes/C_{30} hopane vs C_{21-22}/C_{27-29} steranes and **(B)** Ph/n-C_{18} vs Pr/n-C_{17} (after Shanmugam 1985), showing the depositional condition of the Jurassic organic-rich shale in the East Fukang Sag, Junggar Basin, China.

conditions for the J_1b were suboxic and J_1s were reducing. In summary, the J_2x Formation was deposited under oxic conditions, while J_1 formations developed under suboxic and reducing environmental conditions. This result is completely inconsistent with the previous result based on elements (i.e., Ni/Co, V/Cr, and (Cu+Mo)/Zn) indicating the indiscriminately paleoredox conditions of oxic to dysoxic were prevailing during the deposition of these sediments (Qiao et al., 2020), which reaffirms the need for caution when using elements to identify paleoredox conditions (Algeo and Li, 2020; Algeo and Liu, 2020).
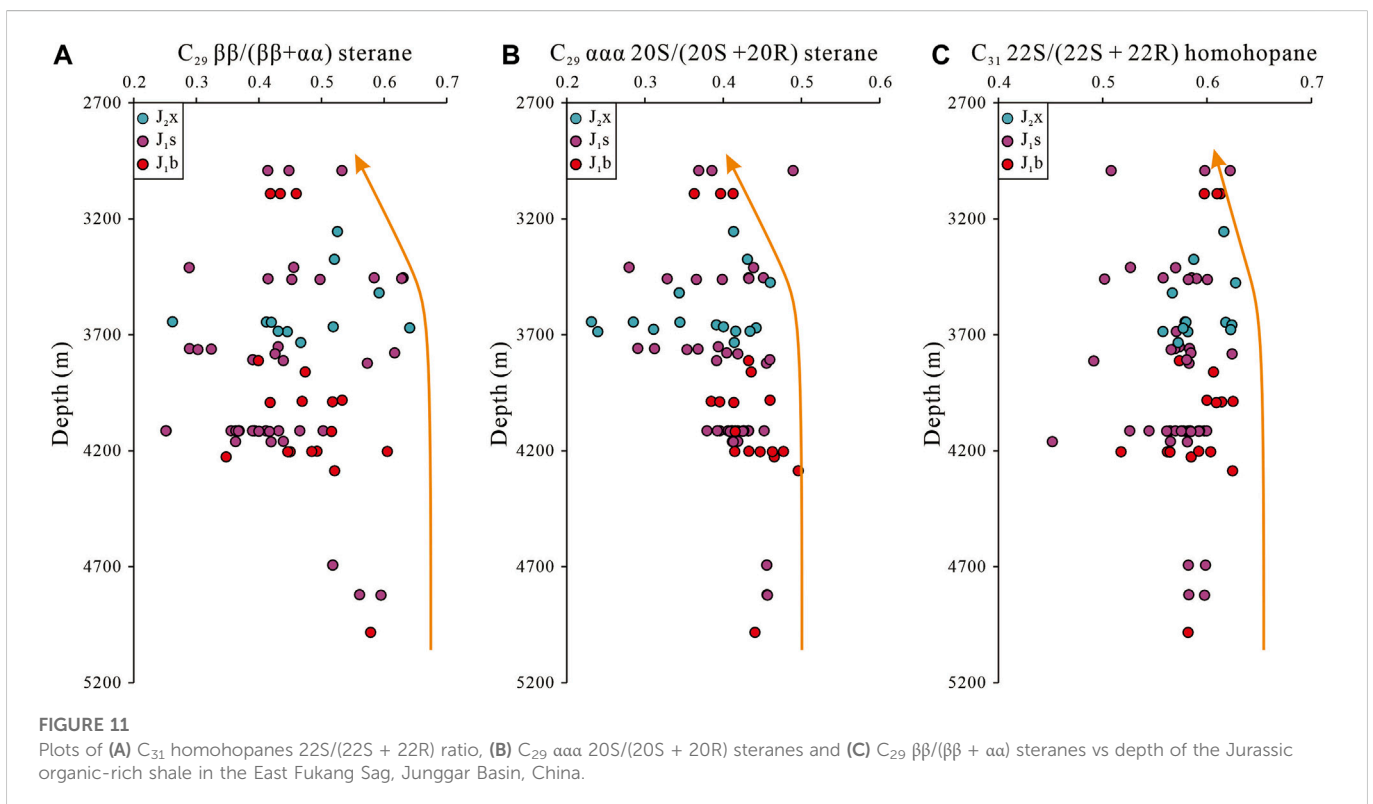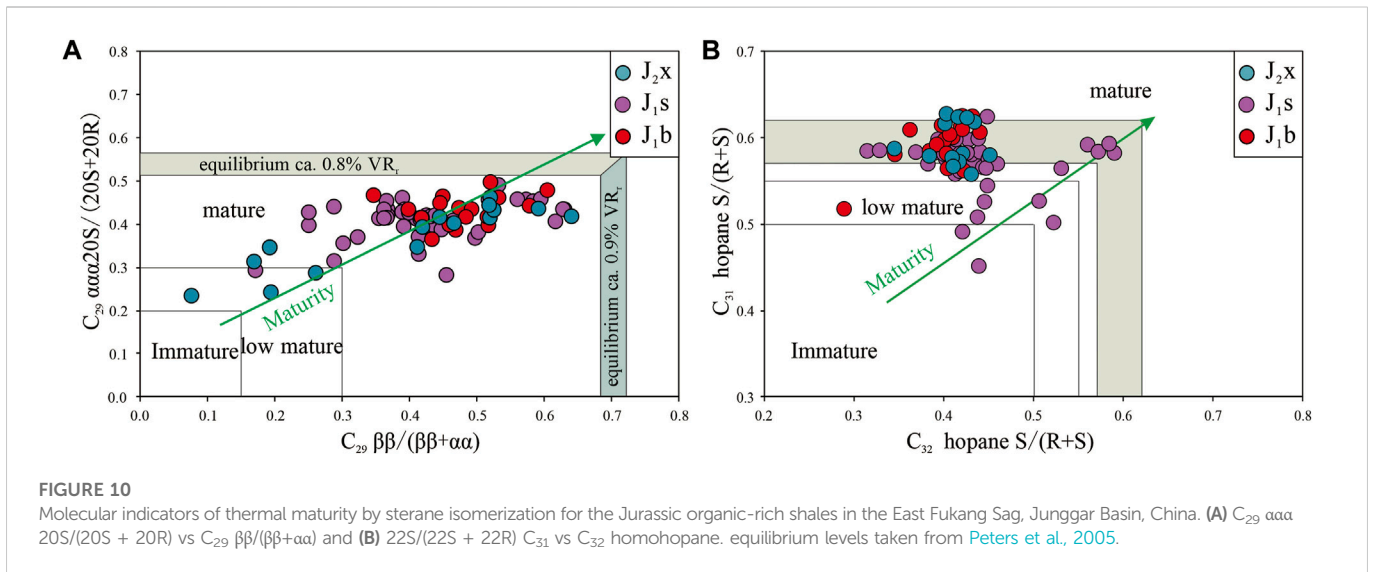
Previous studies have shown that high extended Tri ratios (ETR; (C_{28} Tris + C_{29} Tris)/Ts) are related to the upward shift of the photic zone euxinia caused by water level rise (Pagès et al., 2016), high salinity and strong reducing environments with low terrigenous input (Hao et al., 2009; 2011), or marine upwelling environment (Holba et al., 2001), and the moderate is indicative of an algal contribution of primary producers (Volk et al., 2005). C_{28} and C_{29} Tris can be identified in only two samples of the 15 samples from the J_2x Formation (0.14 and 1.98), but they can be identified in half of the samples from the J_1 formations (0.17–4.77 with an average value of 1.23). Summarizing the above discussions, the variations of ETR values were caused by the large variations of salinity and OM composition predominated by the terrestrial higher plant in all samples but J_2x and J_1 formations formed under different paleoredox conditions.

4.3 Thermal maturity of OM and hydrocarbon potential

Thermal maturity is an essential parameter for shale, which determines whether shale resources are available and what type of shale resources they are (e.g., shale-oil and shale-gas), and shows impacts on the diagenesis and porosity (Liu et al., 2022).

Some molecular parameters are widely used to evaluate thermal maturity (Holba et al., 2003; Volk et al., 2005; Zhu et al., 2012). The R configuration on the side chain of some compounds can be converted to S configuration with the increase of thermal maturity, and finally reached an equilibrium mixture of S and R configurations, thereby being regarded as maturity-dependent ratios,
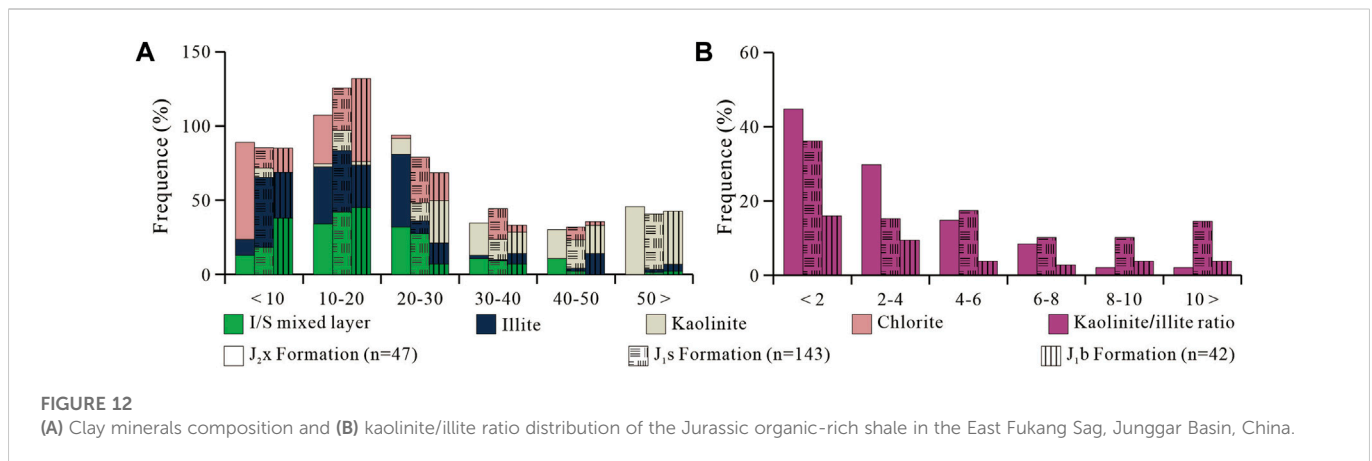
e.g., C_{31} and C_{32} homohopanes 22S/(22S + 22R) ratios as well as C_{29} ααα 20S/(20S + 20R) steranes. Moreover, the stability of a flat three-dimensional configuration (i.e., ααα configuration) is poor, which will transit to a more thermodynamically stable αββ configuration until ααα and αββ configurations reach an equilibrium ratio with the increase of maturity. So, C_{29} ββ/(ββ + αα) steranes can be regarded as a maturity-dependent parameter. Molecular maturity-related parameters are easily affected by conditions of sedimentary water columns. For example, ratios of 22S/(22S + 22R) hopanes and ββ/(ββ + αα) steranes show a higher maturity stage in immature extracts from hypersaline rocks (ten Haven et al., 1986; Rullkötter et al., 1994). This discrepancy can be observed in the Pleistocene hypersaline sediments in the Qaidam Basin, i.e., the obviously too high hopane and steranes maturity-dependent ratios in the definitely immature sediments (Qiao et al., 2021b). Moreover, sterane isomerization ratios are also affected by biodegradation and weathering (Peters et al., 2005). For the analyzed Jurassic shales, there is no clear weathering and biodegradation occurred. Moreover, the salinity of the water columns showed large variation, but it did not develop hypersaline conditions, so the molecular parameters are effective in the study area. A comparison of C_{31} and C_{32} homohopanes 22S/(22S + 22R) ratios being 0.45–0.63 and 0.29–0.59, respectively, indicate a thermal maturity between the early and main oil window (Figure 10A; Peters et al., 2005). The C_{29} ααα 20S/(20S + 20R) (0.23–0.50) vs ββ/(ββ + αα) (0.08–0.64) steranes plot shows similar maturity conditions (Figure 10B; Peters et al., 2005). It should be noted that two samples from J_2x samples are immature based on Figure 10B, which might be because interference by co-eluting peaks can make the homohopane parameters invalid (Peterset al., 2005). The plots of C_{31} homohopanes 22S/(22S + 22R) ratio, C_{29} ααα 20S/(20S + 20R) steranes and C_{29} ββ/(ββ + αα) steranes vs depth (Figure 11) indicate that all the samples' thermal maturity has entered oil windows and the molecular parameters appear to have reached the equilibrium value at around 3,500 m. Furthermore, the thermal maturity is further supported by the CPI (carbon preference index; Bray and Evans 1961) and OEP (odd-to-even predominance; Peters and Moldowan 1993) values. These two parameters are easily affected by the origin of OM because there is no clear odd-to-even predominance in the middle and long chains in the marine algae/saltwater algae.

FIGURE 10
Molecular indicators of thermal maturity by sterane isomerization for the Jurassic organic-rich shales in the East Fukang Sag, Junggar Basin, China. **(A)** C_{29} ααα 20S/(20S + 20R) vs C_{29} ββ/(ββ+αα) and **(B)** 22S/(22S + 22R) C_{31} vs C_{32} homohopane. equilibrium levels taken from Peters et al., 2005.

FIGURE 11
Plots of **(A)** C_{31} homohopanes 22S/(22S + 22R) ratio, **(B)** C_{29} ααα 20S/(20S + 20R) steranes and **(C)** C_{29} ββ/(ββ + αα) steranes vs depth of the Jurassic organic-rich shale in the East Fukang Sag, Junggar Basin, China.

Considering the composition of the OM in the studied samples, the CPI of 1.01–1.43 and OEP of 0.83–1.38 are valid maturity parameters, indicating that most samples have entered into the oil window. The maturity that has entered the oil window is further confirmed by the high saturate/aromatic ratios (0.11–21.84) (Figure 5; Peters et al., 2005) and low to middle percentages of the resins compared to the saturated and aromatic hydrocarbons (from 2.3% to 46.5%, of EOM) (Ayinla et al., 2017). A similar maturity is interpreted by the MPs distribution (Radke, 1983) and the relative abundance of C_{26} and C_{28} 20S triaromatic steroid

(Thompson-Butler et al., 2019) (Figures 3E,H). The above results are consistent with the thermal maturity ranging from low mature and mature supported by Rock-Eval T_{max} (426°C–468°C) and vitrinite reflectance (0.47–1.59%VR_r) values released by Qiao et al. (2020).

Generally, the high PI values are caused by the early generation of hetero-compounds at the lower maturity (Curiale 1986), which are decreasing with the increase of thermal maturity (Lewan 1994). For the studied samples, a small number of samples have high PI values of > 0.4 with relatively lower T_{max} values (Qiao et al., 2020), which are located in the area of the poorly-drained system where hydrocarbons can be

FIGURE 12
(A) Clay minerals composition and (B) kaolinite/illite ratio distribution of the Jurassic organic-rich shale in the East Fukang Sag, Junggar Basin, China.

impregnated in the coarser particle grained laminae in the shale (Jarvie 2012; Li et al., 2018). The relationship between PI and T_{max} values (cf. Figure 4B in Qiao et al., 2020) indicates most analyzed samples are well-drained source rocks which expelled generated hydrocarbons efficiently to the various types of coarser grained siltstone closed intervals (Figure 2) (Raji et al., 2015). This assemblage of shale and siltstone is more typical of the hydrocarbon resources in the Chang 7 Member where coarser intervals (i.e., siltstone/muddy-siltstone) occurred in the direct vicinity within the shaly intervals act as tight-oil reservoirs and the shaly intervals are important shale-oil reservoirs (Qiao et al., 2021a). The economic hydrocarbon potential for the tight-oil reservoirs and shale-oil reservoirs can be further supported by the high oil saturation and the wide range of porosity from the EF 2 well (Figure 2).

4.4 Paleoclimate conditions

Kaolinite formed at temperatures higher than 15°C is commonly found in well-drained soils with high precipitation under humid tropical climates (Egger et al., 2002; John et al., 2012), whereas illite is generally formed in climates with very low weathering rates, such as cold regions and desert areas. Although sea level change and rainfall may also affect kaolinite deposition (e.g., Gibson et al., 2000), climate change is considered to be the primary control for clay minerals composition due to the lack of correlation between sea level change and kaolinite content (e.g., Robert and Chamley, 1991; Bolle and Adatte, 2001). Besides climate conditions, burial diagenesis affects clay mineral composition. Conversion occurs between different clay minerals due to the increase in formation pressure and geotemperature as well as the release of water between clay mineral layers and the migration of interlayer cations. Under shallow burial conditions, kaolinite and smectite exist in clay minerals, but these minerals disappear and are converted to illite and chlorite under deep burial conditions. Considering that the thermal maturity of the examined samples corresponds to the early stage of the intermediate diagenetic stage, the content of kaolinite is much greater than that of illite (Figure 12A), which is sufficient to indicate that the paleoclimate conditions of the study area were warm and humid, although the transition to illite has happened and the transition to chlorite has just begun at this stage as well as how much of these transitions have occurred is uncertain. Moreover, the kaolinite/illite ratio is significantly lower in the J_2x samples compared to that in the J_1 samples (Figure 12B), implying that the paleoclimate conditions were colder and drier during the J_2x period,

which is consistent with the results based on elemental Sr/Cu ratios (cf. Figure 6 in Qiao et al., 2020). This paleoclimatic change is also supported by the lithologic assemblages, i.e., the coal seam is mainly distributed in the J_1b Formation and the lower part of the J_2x Formation (Figure 2). The above inferences are consistent with the interglacial period that occurred during the Jurassic in NW China (Sellwood and Valdes, 1997). The same results were supported by sedimentologic, paleocurrent, and subsidence analyses (Hendrix et al., 1992), lithology characteristics and palynology (Ashraf et al., 2010), as well as sequence stratigraphy characteristics and fossil vertebrates (Eberth et al., 2001; Li et al., 2014).

The change of paleoclimate in the formation of shale is mainly reflected in the water environment and biological composition. The colder and drier paleoclimate conditions may result in a smaller scale of the lake basin and shallower water depth during the J_2x period. This resulted in the oxic benthic water column condition (Figure 9B and discussion in Section 4.2.2) and the proportion of terrestrial higher plants in the OM composition increased (Figure 6 and discussion in Section 4.1) during the J_2x period in comparison to those during the J_1 period. Another important indicator showing the J_2x period was cooler than the J_1 period is β-Carotane which occurs only in the J_2x Formation (Jiang and Fowler, 1986; Fu et al., 1990; Koopmans et al., 1997) although β-Carotane is not very common.

The humid and warm climate conditions during the J_1b, J_1s and J_2x periods of the study area were conducive to the development of the terrestrial higher plant but hard to form brackish water conditions. Even though the studied area became colder and drier during the J_2x period, the change was not significant enough to cause the change of salinity in the water column and the vanish of terrestrial higher plants during the corresponding period (see Section 4.4 and cf; Qiao et al., 2020). Similar paleodepositional conditions can be observed in the Triassic Ordos Basin which developed a mixed OM composition and oxic to suboxic but freshwater conditions (Qiao et al., 2021a). Moreover, it is noteworthy that these salinities did not vary regularly in space and time, showing that they were not affected by climate change, so this variation was more likely due to seawater intrusion as proposed by Sha et al. (2011).

4.5 Enrichment mechanisms of organic-rich shales

Generally, the scale and enrichment degree of shales are controlled by the input and preservation condition of OM, which includes

multiple factors, such as climate, paleontology growth, subsidence rate, as well as level and maturity of lake (Shen et al., 2015; Liu et al., 2021). All of these can be categorized into two groups, i.e., paleoproductivity and depositional conditions (Katz, 2001).

Based on the elemental evaluation proposed by Qiao et al. (2020), the investigated study area developed middle to high productivity. Moreover, the paleoproductivity during the J_1 period was higher than that during the J_2x period based on Ba concentrations (cf. Figure 6 in Qiao et al., 2020), but the TOC contents show similar characteristics vertically in all formations (Figure 2). This is because the Ba concentration only indicates the level of organic carbon fluxes in water columns, while the OM of the J_2x is sourced mainly from terrestrial OM and the redox conditions were oxygen-rich conditions which were not prone to the OM preservation. Based on the relationship between the $\delta^{13}C_{org}$ and TOC content, the OM accumulation was controlled by paleoproductivity in the EF 2 well which is located at the margin of the sag, whereas the redox conditions exerted a primary control on the TOC contents in the samples from the EF 7 well located at the more central area of the sag (cf. Figure 13 in Qiao et al., 2020). This is because the basin margin was more prone to obtain OM from terrestrial higher plants, but the water was shallower and more oxidized due to a reduction in the size of the lake basin caused by cooler and drier paleoclimate conditions, which experienced strong oxygenolysis and were not in favor of the OM preservation. Although the substantial OM input from terrestrial inputs can promote the palaeoproductivity in the sag margin, this input was discontinuous resulting in the large variation of TOC content in the EF 2 well. Therefore, the large variations in the biotic palaeoproductivity from the terrestrial organisms were the material basis controlling the development of the organic-rich shales. By contrast, the redox conditions were more important for controlling OM presentation in the central area of the sag which was far from the terrestrial OM source with a small variation in TOC content (cf. Figure 13 in Qiao et al., 2020). In the central region of the basin, the paleoredox conditions of the benthic water column were deeper and more reductive and were less affected by the reduction of lake scale caused by the paleoclimate change. Considering the accumulation model deduced by Qiao et al. (2020), the paleoredox and salinity conditions as well as OM composition obtained in this study are more reasonable and supply more evidence.

5 Conclusion

The thermal maturity and origins of organic matter (OM), paleodepositional environment, paleoclimate condition, and factors controlling OM accumulation in the J_1b, J_1s and J_2x lacustrine shales in the East Fukang Sag are reassessed by evaluating the organic geochemical characteristics of the OM. Some previous knowledge is updated, and some is further supported by more evidence.

The typical clay-rich shale developed under a lacustrine sedimental environment is recognized. The thermal maturity of these organic-rich shale has entered the oil window and the studied formations have economic hydrocarbon potential for the tight-oil reservoirs and shale-oil reservoirs. The clay minerals compositions and the distribution characteristics of β-Carotane indicate that the paleoclimate conditions of the study area were warm and humid from the Early to Middle Jurassic periods and were colder and drier after the Middle Jurassic period. The lacustrine

environment developed changeable salinity ranging from freshwater to brackish, which is consistent with the reassessment from B/Ga and Sr/Ba ratios based on the update thresholds. The J_2x formation was formed under oxic conditions, while J_1b and J_1s formations were developed under suboxic and reducing environmental conditions. For the OM composition, terrestrial OM and aquatic macrophytes made an important contribution and substantial contribution from bacteria, but the input from algae was limited. For the detail, the J_2x Formation OM originated mainly from higher plants and was deposited in a terrestrial environment, while the OM of J_1b and J_1s formations was a mixed OM derived from higher plants and bacteria with little algae deposited under bay/estuary environments alternated with the terrestrial environment. Using elements to interpret paleoclimate and update elemental thresholds to evaluate paleosalinity conditions are effective, while using common elemental ratios to interpret paleoredox conditions and using Ba to evaluate paleoproductivity are invalid in the studied area.

Data availability statement

The datasets presented in this study can be found in online repositories. The names of the repository/repositories and accession number(s) can be found in the article/Supplementary Material.

Author contributions

Funding

Acknowledgments

Conflict of interest

TZ was employed by the company Xinjiang Oilfield Company.

The remaining authors declare that the research was conducted in the absence of any commercial or financial relationships that could be construed as a potential conflict of interest.

Publisher's note

All claims expressed in this article are solely those of the authors and do not necessarily represent those of their affiliated organizations, or those of the publisher, the editors and the reviewers. Any product that may be evaluated in this article, or claim that may be made by its manufacturer, is not guaranteed or endorsed by the publisher.

References

Algeo, T. J., and Li, C. (2020). Redox classification and calibration of redox thresholds in sedimentary systems. *Geochim. Cosmochim. Acta* 287 (15), 8–26. doi:10.1016/j.gca.2020.01.055

Algeo, T. J., and Liu, J. S. (2020). A re-assessment of elemental proxies for paleoredox analysis. *Chem. Geol.* 540, 119549. doi:10.1016/j.chemgeo.2020.119549

Algeo, T. J., and Maynard, J. B. (2004). Trace-element behavior and redox facies in core shales of Upper Pennsylvanian Kansas-type cyclothems. *Chem. Geol.* 206 (3-4), 289–318. doi:10.1016/j.chemgeo.2003.12.009

Arsairai, B., Wannakomol, A., Feng, Q. L., and Chonglakmani, C. (2016). Paleoproductivity and paleoredox condition of the huai hin lat formation in northeastern Thailand. *J. Earth Sci.* 27 (3), 350–364. doi:10.1007/s12583-016-0666-8

Ashraf, A. R., Sun, Y., Sun, G., Uhl, D., Mosbrugger, V., Li, J., et al. (2010). Triassic and jurassic palaeoclimate development in the Junggar Basin, Xinjiang, northwest China—A review and additional lithological data. *Palaeobio. Palaeoenv.* 90 (3), 187–201. doi:10.1007/s12549-010-0034-0

Ayinla, H. A., Abdullah, W. H., Makeen, Y. M., Abubakar, M. B., Jauro, A., Yandoka, B. M. S., et al. (2017). Source rock characteristics, depositional setting and hydrocarbon generation potential of Cretaceous coals and organic rich mudstones from Gombe Formation, Gongola Sub-basin, Northern Benue Trough, NE Nigeria. *Int. J. Coal Geol.* 173, 212–226. doi:10.1016/j.coal.2017.02.011

Bian, W., Hornung, J., Liu, Z., Wang, P., and Hinderer, M. (2010). Sedimentary and palaeoenvironmental evolution of the Junggar Basin, Xinjiang, northwest China. *Palaeobio. Palaeoenv.* 90 (3), 175–186. doi:10.1007/s12549-010-0038-9

Bingham, E. M., McClymont, E. L., Valiranta, M., Mauquoy, D., Roberts, Z., Chambers, F. M., et al. (2010). Conservative composition of n-alkane biomarkers in Sphagnum species: Implications for palaeoclimate reconstruction in ombrotrophic peat bogs. *Org. Geochem.* 41 (2), 214–220. doi:10.1016/j.orggeochem.2009.06.010

Bolle, M. P., and Adatte, T. (2001). Palaeocene early eocene climatic evolution in the tethyan realm: Clay mineral evidence. *Clay Min.* 36, 249–261. doi:10.1180/000985501750177979

Bray, E. E., and Evans, E. D. (1961). Distribution of n-paraffins as a clue to recognition of source beds. *Geochim. Cosmochim. Acta* 22, 2–15. doi:10.1016/0016-7037(61)90069-2

Cao, B., Luo, X., Zhang, L., Sui, F., Lin, H., and Lei, Y. (2017b). Diagenetic evolution of deep sandstones and multiple-stage oil entrapment: A case study from the lower jurassic sangonghe formation in the Fukang sag, central Junggar Basin (NW China). *J. Pet. Sci. Eng.* 152, 136–155. doi:10.1016/j.petrol.2017.02.019

Cao, B., Luo, X., Zhang, L., Sui, F., Lin, H., and Lei, Y. (2017a2017). Diagenetic heterogeneity of deep sandstones and its relationship to oil emplacement: A case study from the middle jurassic toutunhe formation in the Fukang sag, central Junggar Basin (NW China). *Geofluids* 2017, 1–23. doi:10.1155/2017/4292079

Cao, J., Zhang, Y., Hu, W., Yao, S., Wang, X., Zhang, Y., et al. (2005). The Permian hybrid petroleum system in the northwest margin of the Junggar Basin, northwest China. *Mar. Pet. Geol.* 22 (3), 331–349. doi:10.1016/j.marpetgeo.2005.01.005

Cao, L., Zhang, Z., Zhao, J., Jin, X., Li, H., Li, J., et al. (2021). Discussion on the applicability of Th/U ratio for evaluating the paleoredox conditions of lacustrine basins. *Int. J. Coal Geol.* 248, 103868. doi:10.1016/j.coal.2021.103868

Chaffee, A. L., and Fookes, C. J. R. (1988). Polycyclic aromatic hydrocarbons in Australian coals—III, structural elucidation by proton nuclear magnetic resonance spectroscopy. *Org. Geochem.* 12, 261–271. doi:10.1016/0146-6380(88)90263-X

Chaffee, A. L., and Johns, R. B. (1983). Polycyclic aromatic hydrocarbons in Australian coals, I. Angularly fused pentacyclic tri-and tetraaromatic components of Victorian Brown coal. *Geochim. Cosmochim. Acta* 47, 2141–2155. doi:10.1016/0016-7037(83)90039-X

Chen, J. B., Thomas, A. D., Zhao, L. S., Chen, Z. Q., Cao, L., Zhang, L., et al. (2015a). Diagenetic uptake of rare Earth elements by biopatite, with an example from Lower Triassic conodonts from South China. *Earth-Sci. Rev.* 149, 181–202. doi:10.1016/j.earscirev.2015.01.013

Chen, J., Deng, C., Liang, D., Wang, X., Zhong, N., Song, F., et al. (2003a). Mixed oils derived from multiple source rocks in the cainan oilfield, Junggar Basin, northwest China. Part II: Artificial mixing experiments on typical crude oils and quantitative oil–source correlation. *Org. Geochem.* 34 (7), 911–930. doi:10.1016/S0146-6380(03)00031-7

Chen, J., Liang, D., Wang, X., Zhong, N., Song, F., Deng, C., et al. (2003b). Mixed oils derived from multiple source rocks in the cainan oilfield, Junggar Basin, northwest China. Part I: Genetic potential of source rocks, features of biomarkers and oil sources of typical crude oils. *Org. Geochem.* 34 (7), 889–909. doi:10.1016/S0146-6380(03)00030-5

Chen, Z. Q., Liao, Z. T., and Liu, L. J. (2015b). Correction of two upper paleozoic stratigraphic units in the tianshan mountains region, Xinjiang uygur autonomous region

and implications on the late paleozoic evolution of tianshan tectonic complex, northwest China. *J. Paleogeog.-English.* doi:10.1016/j.jop.2015.05.001

Chen, Z. Q., and Shi, G. R. (2003). Late Paleozoic depositional history of the Tarim basin, northwest China: An integration of biostratigraphic and lithostratigraphic constraints. *AAPG Bull.* 87, 1323–1354. doi:10.1306/0401032001115

Cheng, D. W., Zhou, C. M., Zhang, Z. J., Yuan, X. J., Liu, Y. H., and Chen, X. Y. (2022). Paleo-environment reconstruction of the middle permian lucaogou formation, southeastern Junggar Basin, NW China: Implications for the mechanism of organic matter enrichment in ancient lake. *J. Earth Sci.* 33 (4), 963–976. doi:10.1007/s12583-020-1073-8

Choi, J. H., and Hariya, Y. (1992). Geochemistry and depositional environment of Mn oxide deposits in the Tokoro Belt, northeastern Hokkaido. Japan. *J. Econ. Geol.* 87 (5), 1265–1274. doi:10.2113/gsecongeo.87.5.1265

Coetzee, J. A. (1967). Pollen analytical studies in east and southern africa. *Palaeoecology* 3, 1–146. doi:10.1177/0309133307079056

Collister, J. W., and Wavrek, D. A. (1996). ^{13}C compositions of saturate and aromatic fractions of lacustrine oils and bitumens: Evidence for water column stratification. *Org. Geochem.* 24, 913–920. doi:10.1016/S0146-6380(96)00066-6

Curiale, J. A. (1986). Origin of solid bitumens, with emphasis on biological marker results. *Org. Geochem.* 10, 559–580. doi:10.1016/0146-6380(86)90054-9

Didyk, B. M., Simoneit, B. R. T., Brassell, S. C., and Eglinton, G. (1978). Organic geochemical indicators of palaeoenvironmental conditions of sedimentation. *Nature* 272, 216–222. doi:10.1038/272216a0

Eberth, D. A., Brinkman, D. B., Chen, P. J., Yuan, F. T., Wu, Z., Li, G., et al. (2001). Sequence stratigraphy, paleoclimate patterns, and vertebrate fossil preservation in jurassic cretaceous strata of the Junggar Basin, Xinjiang autonomous region, people's republic of China. *Can. J. Earth Sci.* 38 (12), 1627–1644. doi:10.1139/e01-067

Egger, H., Homayoun, M., and Schnabel, W. (2002). Tectonic and climatic control of Paleogene sedimentation in the Rhenodanubian Flysch basin (eastern Alps, Austria). *Sediment. Geol.* 152, 247–262. doi:10.1016/S0037-0738(02)00072-6

Eglinton, G., and Calvin, M. (1967). Chemical fossils. *Sci. Am.* 216 (1), 32–43. doi:10.1038/scientificamerican0167-32

El Diasty, W. S., El Beialy, S. Y., Mahdi, A. Q., and Peters, K. E. (2016). Geochemical characterization of source rocks and oils from northern Iraq: Insights from biomarker and stable carbon isotope investigations. *Mar. Pet. Geol.* 77, 1140–1162. doi:10.1016/j.marpetgeo.2016.07.019

Ficken, K. J., Li, B., Swain, D. L., and Eglinton, G. (2000). An n-alkane proxy for the sedimentary input of submerged/floating freshwater aquatic macrophytes. *Org. Geochem.* 31 (7–8), 745–749. doi:10.1016/S0146-6380(00)00081-4

Fu, J., Sheng, G., Xu, J., Eglinton, G., Gowar, A., Rongfen, J., et al. (1990). Application of biological markers in the assessment of paleoenvironments of Chinese non-marine sediments. *Org. Geochem.* 16, 769–779. doi:10.1016/0146-6380(90)90116-H

Galimov, E. M. (2006). Isotope organic geochemistry. *Org. Geochem.* 37, 1200–1262. doi:10.1016/j.orggeochem.2006.04.009

Gibson, T. G., Bybell, L. M., and Mason, D. B. (2000). Stratigraphic and climatic implications of clay mineral changes around the Paleocene/Eocene boundary of the northeastern US margin. *Sediment. Geol.* 134, 65–92. doi:10.1016/S0037-0738(00)00014-2

Gonzales, L. D., Mastalerz, M., and Mendonca Filho, J. G. (2020). Application of organic facies and biomarkers in characterization of paleoenvironmental conditions and maturity of sediments from the Codo Formation in the west central part of the Sao Luis Basin, Brazil. *Int. J. Coal Geol.* 225, 103482. doi:10.1016/j.coal.2020.103482

Gürgey, K. (1999). Geochemical characteristics and thermal maturity of oils from the Thrace Basin (Western Turkey) and Western Turkmenistan. *J. Pet. Geol.* 22 (2), 167–189. doi:10.1111/j.1747-5457.1999.tb00466.x

Hao, F., Zhou, X., Zhu, Y., and Yang, Y. (2011). Lacustrine source rock deposition in response to co-evolution of environments and organisms controlled by tectonic subsidence and climate, Bohai Bay Basin, China. *Org. Geochem.* 42, 323–339. doi:10.1016/j.orggeochem.2011.01.010

Hao, F., Zhou, X., Zhu, Y., and Yang, Y. (2009). Mechanisms for oil depletion and enrichment on the shijiutuo uplift, Bohai Bay Basin, China. *AAPG Bull.* 93, 1015–1037. doi:10.1306/04140908156

Hendrix, M. S., Graham, S. A., Carroll, A. R., Sober, E. R., McKnight, C. L., Shulein, B. J., et al. (1992). Sedimentary record and climatic implications of recurrent deformation in the Tian Shan: Evidence from Mesozoic strata of the north Tarim, south Junggar, and Turpan basins, northwest China. *Geol. Soc. Am. Bull.* 104, 53–79. doi:10.1130/0016-7606(1992)104<0053:sracio>2.3.co;2

Holba, A. G., Dzou, L. I., Wood, G. D., Ellis, L., Adam, P., Schaeffer, P., et al. (2003). Application of tetracyclic polyprenoids as indicators of input from fresh-brackish water environments. *Org. Geochem.* 34, 441–469. doi:10.1016/S0146-6380(02)00193-6

Holba, A. G., Ellis, L., Dzou, L. I., Hallam, A., Masterson, W. D., Francu, J., et al. (2001). "Extended tricyclic terpanes as age discriminators between Triassic, early Jurassic, and Middle–Late Jurassic oils," in *20th international meeting on organic geochemistry* (France: Nancy), 464.

Huang, W. Y., and Meinschein, W. G. (1979). Sterols as ecological indicators. *Geochim. Cosmochim. Acta* 43 (5), 739–745. doi:10.1016/0016-7037(79)90257-6

Huang, Y. S., Street-Perrott, F. A., Perrott, R. A., Metzger, P., and Eglinton, G. (1999). Glacial-interglacial environmental changes inferred from molecular and compound-specific δ13C analyses of sediments from Sacred Lake, Mt. Kenya. *Geochim. Cosmochim. Acta* 63 (9), 1383–1404. doi:10.1016/s0016-7037(99)00074-5

Jarvie, D. M. (2012). Shale resource systems for oil and gas: Part 1—shale-gas resource systems. *Am. Assoc. Pet. Geol. Mem.* 97, 69–87. doi:10.1306/13321446M973489

Jiang, Z., and Fowler, M. G. (1986). Carotenoid-derived alkanes in oils from northwestern China. *Org. Geochem.* 10, 831–839. doi:10.1016/S0146-6380(86)80020-1

John, C. M., Banerjee, N. R., Longstaffe, F. J., Sica, C., Law, K. R., and Zachos, J. C. (2012). Clay assemblage and oxygen isotopic constraints on the weathering response to the Paleocene-Eocene thermal maximum, East Coast of North America. *Geol* 40, 591–594. doi:10.1130/G32785.1

Johnsson, M. J. (1993). "The system controlling the composition of clastic sediments,". Editors M. J. Johnsson and A. Basu *Process. Control. Compos. clastic sediments.* (Colorado: Geol. Soc. Am., Spec. Pap), 284, 1–19. doi:10.1130/SPE284-p1

Jones, B., and Manning, D. A. C. (1994). Comparison of geochemical indices used for the interpretation of palaeoredox conditions in ancient mudstones. *Chem. Geol.* 111 (1-4), 111–129. doi:10.1016/0009-2541(94)90085-X

Katz, B. J. (2001). Lacustrine basin hydrocarbon exploration–current thoughts. *J. Paleolimnol.* 26 (2), 161–179. doi:10.1023/A:1011173805661

Koopmans, M. P., de Leeuw, J. W., and Sinninghe Damsté, J. S. (1997). Novel cyclised and aromatised diagenetic products of β-carotene in the Green River Shale. *Org. Geochem.* 26, 451–466. doi:10.1016/S0146-6380(97)00025-9

Kruge, M. A., Hubert, J. F., Bensley, D. F., Crelling, J. C., Akes, R. J., and Meriney, P. E. (1990). Organic geochemistry of a lower jurassic synrift lacustrine sequence, Hartford Basin, Connecticut, U.S.A. *Org. Geochem.* 16, 689–701. doi:10.1016/0146-6380(90)90110-L

Lewan, M. D. (1994). "Assessing natural oil expulsion from source rocks by laboratory pyrolysis,". Editors L. B. Magoon and W. G. Dow *Petroleum Syst. – Source Trap.* (Oklahoma: AAPG Memoir), 60, 201–210. doi:10.1306/M60585C11

Li, M. W., Chen, Z. H., Cao, T. T., Ma, X., Liu, X., Li, Z., et al. (2018). Expelled oils and their impacts on rock-eval data interpretation, Eocene Qianjiang Formation in Jianghan Basin, China. *Int. J. Coal Geol.* 191, 37–48. doi:10.1016/j.coal.2018.03.001

Li, S. L., Yu, X. H., Tan, C. P., Steel, R., and Hu, X. F. (2014). Jurassic sedimentary evolution of southern Junggar Basin: Implication for palaeoclimate changes in northern Xinjiang Uygur Autonomous Region, China. *J. Palaeogeogr.* 3 (2), 145–161. doi:10.3724/SP.J.1261.2014.00049

Liu, B., Song, Y., Zhu, K., Su, P., Ye, X., and Zhao, W. (2020). Mineralogy and element geochemistry of salinized lacustrine organic-rich shale in the Middle Permian Santanghu Basin: Implications for paleoenvironment, provenance, tectonic setting and shale oil potential. *Mar. Pet. Geol.* 120, 104569. doi:10.1016/j.marpetgeo.2020.104569

Liu, B., Wang, Y., Tian, S., Guo, Y., Wang, L., Yasin, Q., et al. (2022). Impact of thermal maturity on the diagenesis and porosity of lacustrine oil-prone shales: Insights from natural shale samples with thermal maturation in the oil generation window. *Int. J. Coal Geol.* 261, 4079. doi:10.1016/j.coal.2022.104079

Liu, Q. Y., Li, P., Jin, Z. J., Liang, X. P., Zhu, D. Y., Wu, X. Q., et al. (2021). Preservation of organic matter in shale linked to bacterial sulfate reduction (BSR) and volcanic activity under marine and lacustrine depositional environments. *Mar. Pet. Geol.* 127, 104950. doi:10.1016/j.marpetgeo.2021.104950

Luo, Q. Y., George, S. C., Xu, Y. H., and Zhong, N. (2016). Organic geochemical characteristics of the Mesoproterozoic Hongshuizhuang Formation from northern China: implications for thermal maturity and biological sources. *Org. Geochem.* 9923– 99, 23–37. doi:10.1016/j.orggeochem.2016.05.004

McLennan, S. M. (1993). Weathering and global denudation. *Geol. J.* 101 (2), 295–303. doi:10.1086/648222

Meyers, P. A. (1997). Organic geochemical proxies of paleoceanographic, paleolimnologic, and paleoclimatic processes. *Org. Geochem.* 27 (5–6), 213–250. doi:10.1016/S0146-6380(97)00049-1

Moldowan, J. M., Seifert, W. K., and Gallegos, E. J. (1985). Relationship between petroleum composition and depositional environment of petroleum source rocks. *AAPG Bull.* 69 (8), 1255–1268. doi:10.1306/AD462BC8-16F7-11D7-8645000102C1865D

Moldowan, J. M., Sundararaman, P., and Schoell, M. (1986). Sensitivity of biomarker properties to depositional environment and/or source input in the Lower Toarcian of SW-Germany. *Org. Geochem.* 10 (4-6), 915–926. doi:10.1016/S0146-6380(86)80029-8

Nichols, J. E., Booth, R. K., Jackson, S. T., Pendall, E. G., and Huang, Y. (2006). Paleohydrologic reconstruction based on n-alkane distributions in ombrotrophic peat. *Org. Geochem.* 37 (11), 1505–1513. doi:10.1016/j.orggeochem.2006.06.020

Oros, D. R., Standley, L. J., Chen, X., and Simoneit, B. R. (1999). Epicuticular wax compositions of predominant conifers of Western North America. *Z. für Naturforsch. C* 54 (1–2), 17–24. doi:10.1515/znc-1999-1-205

Ourisson, G., and Rohmer, M. (1992). Hopanoids. 2. Biohopanoids: a novel class of bacterial lipids. *Acc. Chem. Res.* 25 (9), 403–408. doi:10.1021/ar00021a004

Pagès, A., Schmid, S., Edwards, D., Barnes, S., He, N., and Grice, K. (2016). A molecular and isotopic study of palaeoenvironmental conditions through the middle Cambrian in the Georgina Basin, central Australia. *Earth Planet Sci. Lett.* 447, 21–32. doi:10.1016/j.epsl.2016.04.032

Pan, Y., Sha, J., Wang, Y., Zhang, X., Yao, X., Peng, B., et al. (2013). The brackish-water bivalve Waagenoperna from the Lower jurassic Badaowan Formation of the Junggar Basin and its palaeoenvironmental and palaeogeographic significance. *Geosci. Front.* 4 (1), 95–103. doi:10.1016/j.gsf.2012.05.007

Peters, K. E., and Moldowan, J. M. (1991). Effects of source, thermal maturity, and biodegradation on the distribution and isomerization of homohopanes in petroleum. *Org. Geochem.* 17 (1), 47–61. doi:10.1016/0146-6380(91)90039-M

Peters, K. E., and Moldowan, J. M. (1993). *The biomarker guide: Interpreting molecular fossils in petroleum and ancient sediments.* Englewood Cliffs, NJ: Prentice-Hall.

Peters, K. E., Walters, C. C., and Moldowan, J. M. (2005). *The biomarker guide: Column 2, biomarkers and isotopes in petroleum systems and Earth history.* 2nd Edition. Cambridge: Cambridge University Press. doi:10.1017/CBO9781107326040

Qiao, J., Luo, Q., Zhang, C., and Jiang, Z. (2022b). Geological implications of elements of the Pleistocene mudstone with different organism compositions and enrichment environments in the Qaidam Basin. *China Front. Earth Sci.* doi:10.1007/s11707-022-0996-z

Qiao, J. Q., Baniasad, A., Zieger, L., Zhang, C., Luo, Q., and Littke, R. (2021a). Paleo-depositional environment, origin and characteristics of organic matter of the Triassic Chang 7 Member of the Yanchang Formation throughout the mid-Western part of the Ordos Basin, China. *Int. J. Coal Geol.* 237, 103636. doi:10.1016/j.coal.2020.103636

Qiao, J. Q., Grohmann, S., Baniasad, A., Zhang, C., Jiang, Z. X., and Littke, R. (2021b). High microbial gas potential of Pleistocene lacustrine deposits in the central Qaidam Basin, China: An organic geochemical and petrographic assessment. *Int. J. Coal Geol.* 245, 3818. doi:10.1016/j.coal.2021.103818

Qiao, J. Q., Littke, R., Grohmann, S., Zhang, C., Jiang, Z. X., Strauss, H., et al. (2022a). Climatic and environmental conditions during the Pleistocene in the Central Qaidam Basin, NE Tibetan Plateau: Evidence from GDGTs, stable isotopes and major and trace elements of the Qigequan Formation. *Int. J. Coal Geol.* 254, 103958. doi:10.1016/j.coal.2022.103958

Qiao, J. Q., Liu, L. F., and Shang, X. Q. (2020). Deposition conditions of the jurassic lacustrine source rocks in the East Fukang sag, junggar basin, nw China: evidence from major and trace elements. *Geol. J.* 55 (7), 4936–4953. doi:10.1002/gj.3714

Radke, M. (1983). The methylphenanthrene index (MPI): a maturity parameter based on aromatic hydrocarbons. *Adv. Org. Geochem.* 1981, 504–512. doi:10.3720/japt.60.285

Raji, M., Gröcke, D. R., Greenwell, H. C., Gluyas, J. G., and Cornford, C. (2015). The effect of interbedding on shale reservoir properties. *Mar. Pet. Geol.* 67, 154–169. doi:10.1016/j.marpetgeo.2015.04.015

Riboulleau, A., Schnyder, J., Riquier, L., Lefebvre, V., Baudin, F., and Deconinck, J. F. (2007). Environmental change during the Early Cretaceous in the Purbeck-type Durlston Bay section (Dorset, Southern England): a biomarker approach. *Org. Geochem.* 38 (11), 1804–1823. doi:10.1016/j.orggeochem.2007.07.006

Robert, C., and Chamley, H. (1991). Development of early Eocene warm climates, as inferred from clay mineral variations in oceanic sediments. *Glob. Planet. Chang.* 3, 315–331. doi:10.1016/0921-8181(91)90114-C

Romero-Viana, L., Kienel, U., and Sachse, D. (2012). Lipid biomarker signatures in a hypersaline lake on Isabel Island (Eastern Pacific) as a proxy for past rainfall anomaly (1942–2006 AD). *Palaeogeogr. Palaeoclimatol. Palaeoecol.* 350, 49–61. doi:10.1016/j.palaeo.2012.06.011

Rullkötter, J., Peakman, T. M., and ten Haven, H. L. (1994). Early diagenesis of terrigenous triterpenoids and its implications for petroleum geochemistry. *Org. Geochem.* 21, 215–233. doi:10.1016/0146-6380(94)90186-4

Sachse, D., and Sachs, J. P. (2008). Inverse relationship between D/H fractionation in cyanobacterial lipids and salinity in Christmas Island saline ponds. *Geochim. Cosmochim. Acta* 72 (3), 793–806. doi:10.1016/j.gca.2007.11.022

Schoepfer, S. D., Shen, J., Wei, H., Tyson, R. V., Ingall, E., and Algeo, T. J. (2015). Total organic carbon, organic phosphorus, and biogenic barium fluxes as proxies for paleomarine productivity. *Earth-Sci. Rev.* 149, 23–52. doi:10.1016/j.earscirev.2014.08.017

Sellwood, B. W., and Valdes, P. J. (1997). Geological evaluation of climate General Circulation Models and model implications for Mesozoic cloud cover. *Terra nova.* 9 (2), 75–78. doi:10.1111/j.1365-3121.1997.tb00006.x

Sha, J. G., Vajda, V., Pan, Y. H., Larsson, L., Yao, X. G., Zhang, X. L., et al. (2011). Stratigraphy of the Triassic-Jurassic Boundary Successions of the Southern Margin of the Junggar Basin, Northwestern China. *Acta Geol. Sin.* 85 (2), 421–436. doi:10.1111/j.1755-6724.2011.00410.x

Shanmugam, G. (1985). Significance of Coniferous rain Forests and Related Organic Matter in Generating Commercial Quantities of Oil, Gippsland Basin, Australia1. *AAPG Bull.* 69 (8), 1241–1254. doi:10.1306/AD462BC3-16F7-11D7-8645000102C1865D

Shen, J., Schoepfer, S. D., Feng, Q., Zhou, L., Yu, J., Song, H., et al. (2015). Marine productivity changes during the end-Permian crisis and Early Triassic recovery. *Earth-Sci. Rev.* 149, 136–162. doi:10.1016/j.earscirev.2014.11.002

Shiea, J., Brassell, S. C., and Ward, D. M. (1990). Mid-chain branched mono-and dimethyl alkanes in hot spring cyanobacterial mats: a direct biogenic source for branched alkanes in ancient sediments? *Org. Geochem.* 15 (3), 223–231. doi:10.1016/0146-6380(90)90001-G

Sinninghe Damsté, J. S., Kenig, F., Koopmans, M. P., Köster, J., Schouten, S., Hayes, J. M., et al. (1995). Evidence for gammacerane as an indicator of water column stratification. *Geochim. Cosmochim. Acta* 59 (9), 1895–1900. doi:10.1016/0016-7037(95)00073-9

Sofer, Z. (1984). Stable carbon isotope compositions of crude oils: application to source depositional environments and petroleum alteration. *AAPG Bull.* 68, 31–49. doi:10.1306/AD460963-16F7-11D7-8645000102C1865D

Strobl, S. A., Sachsenhofer, R. F., Bechtel, A., Gratzer, R., Gross, D., Bokhari, S. N., et al. (2014). Depositional environment of oil shale within the Eocene Jijuntun Formation in the Fushun Basin (NE China). *Mar. Pet. Geol.* 56, 166–183. doi:10.1016/j.marpetgeo.2014.04.011

Summons, R. E., and Powell, T. G. (1987). Identification of aryl isoprenoids in source rocks and crude oils: biological markers for the green sulphur bacteria. *Geochim. Cosmochim. Acta* 51 (3), 557–566. doi:10.1016/0016-7037(87)90069-X

ten Haven, H. L., de Leeuw, J. W., Peakman, T. M., and Maxwell, J. R. (1986). Anomalies in steroid and h opanoid maturity indices. *Geochim. Cosmochim. Acta.* 50, 853–855. doi:10.1016/0016-7037(86)90361-3

Thompson-Butler, William., Peters, K. E., Magoon, L. B., Scheirer, A. H., Moldowan, J. M., Blanco, V. O., et al. (2019). Identification of genetically distinct petroleum tribes in the Middle Magdalena Valley, Colombia. *AAPG Bull.* 103 (12), 3003–3034. doi:10.1306/04101918107

Tribovillard, N., Algeo, T. J., Baudin, F., and Riboulleau, A. (2012). Analysis of marine environmental conditions based on molybdenum–uranium covariation—applications to Mesozoic paleoceanography. *Chem. Geol.* 324, 46–58. doi:10.1016/j.chemgeo.2011.09.009

Tribovillard, N. P., Algeo, T. J., Lyons, T., and Riboulleau, A. (2006). Trace metals as paleoredox and paleoproductivity proxies: an update. *Chem. Geol.* 232 (1-2), 12–32. doi:10.1016/j.chemgeo.2006.02.012

Volk, H., George, S. C., Middleton, H., and Schofield, S. (2005). Geochemical comparison of fluid inclusion and present-day oil accumulations in the papuan foreland–evidence for previously unrecognised petroleum source rocks. *Org. Geochem.* 36 (1), 29–51. doi:10.1016/j.orggeochem.2004.07.018

Volkman, J. K. (2003). Sterols in microorganisms. *Appl. Microbiol. Biotechnol.* 60 (5), 495–506. doi:10.1007/s00253-002-1172-8

Wan, Z., Shi, Q., Zhang, Q., Cai, S., and Xia, B. (2015). Characteristics and developmental mechanisms of mud volcanoes on the southern margin of the Junggar Basin, NW China. *Geol. J.* 50 (4), 434–445. doi:10.1002/gj.2547

Wang, G. L., Chang, X. C., Wang, T. G., and Simoneit, B. R. (2015). Pregnanes as molecular indicators for depositional environments of sediments and petroleum source rocks. *Org. Geochem.* 78, 110–120. doi:10.1016/j.orggeochem.2014.11.004

Waseda, A., and Nishita, H. (1998). Geochemical characteristics of terrigenous- and marine-sourced oils in Hokkaido, Japan. *Org. Geochem.* 28 (1–2), 27–41. doi:10.1016/S0146-6380(97)00102-2

Wei, W., and Algeo, T. J. (2020). Elemental proxies for paleosalinity analysis of ancient shales and mudrocks. *Acta* 287, 341–366. doi:10.1016/j.gca.2019.06.034

Wu, J., Li, H., Goodarzi, F., Min, X., Cao, W., Huang, L., et al. (2022a). Geochemistry and depositional environment of the Mesoproterozoic Xiamaling shales, northern North China. *J. Pet. Sci. Eng.* 215, 110730. doi:10.1016/j.petrol.2022.110730

Wu, Z. R., Grohmann, S., Littke, R., Guo, T. X., He, S., and Baniasad, A. (2022b). Organic petrologic and geochemical characterization of petroleum source rocks in the Middle Jurassic Dameigou Formation, Qaidam Basin, northwestern China: Insights into paleo-depositional environment and organic matter accumulation. *Int. J. Coal Geol.* 259, 104038. doi:10.1016/j.coal.2022.104038

Zhang, M. M., Liu, Z. J., Xu, S. C., Sun, P. C., and Hu, X. F. (2013). Element response to the ancient lake information and its evolution history of argillaceous source rocks in the lucaogou formation in sangonghe area of southern margin of junggar basin. *J. Earth Sci.* 24 (6), 987–996. doi:10.1007/s12583-013-0392-4

Zhang, Q., Grohmann, S., Xu, X. C., and Littke, R. (2020). Depositional environment and thermal maturity of the coal-bearing Longtan Shale in southwest Guizhou, China: Implications for shale gas resource potential. *Int. J. Coal Geol.* 231, 103607. doi:10.1016/j.coal.2020.103607

Zheng, T. Y., Zieger, L., Baniasad, A., Grohmann, S., Hu, T., and Littke, R. (2022). The Shahejie Formation in the Dongpu Depression, Bohai Bay Basin, China: Geochemical investigation of the origin, deposition and preservation of organic matter in a saline lacustrine environment during the Middle Eocene. *Int. J. Coal Geol.* 253, 103967. doi:10.1016/j.coal.2022.103967

Zhu, G., Chen, W., Yan, H., Yan, L., Zhang, Z., Zhao, K., et al. (2022). Sinian tectonic evolution and distribution of source rocks in northwest Tarim Basin, China. *Mar. Petroleum Geol.* 144, 105826. doi:10.1016/j.marpetgeo.2022.105826

Zhu, G., Zhang, S., Su, J., Huang, H., Yang, H., Gu, L., et al. (2012). The occurrence of ultra-deep heavy oils in the Tabei Uplift of the Tarim Basin, NW China. *Org. Geochem.* 52, 88–102. doi:10.1016/j.orggeochem.2012.08.012

Zhu, X., Li, S., Wu, D., Zhu, S., Dong, Y., Zhao, D., et al. (2017). Sedimentary characteristics of shallow-water braided delta of the Jurassic, Junggar basin, Western China. *J. Pet. Sci. Eng.* 149, 591–602. doi:10.1016/j.petrol.2016.10.054